Table 1. Optical Resolution of 1a by Lipase Catalysts[a,b]

			ee (%)		
entry	enzyme[c]	time (h)	(*P*)-**1b**[d]	(*M*)-**1a**[d]	*c* (%)
1	Amano PS	24	38	35	59
2	Amano PS IM	4	35	45	59
3	Amano M	18	23	18	56
4	F-Ap 15	48	4	2	51
5	CAL	72	——	——	——
6	Amano AK	72	——	——	——
7	Amano AYS	72	——	——	——
8[e]	Amano PS IM	0.2	76	29	27
9[e]	Amano PS IM	0.5	67	67	51
10[e]	Amano PS IM	1	52	92	65

[a]General conditions: 1 mmol (5 mg) of substrate, 5 mg of lipase in 1 mL of MTBE (0.25% H_2O), 30 °C. [b]The conversion values and enantiomeric excesses were determined by HPLC using a Chiralcel IA column. [c]Amano PS: *Burkholderia cepacia* lipase; Amano M: *Mucor javanicus* lipase; F-Ap 15; *Rhizopus oryzae* lipase; CAL: *Candida antarctica* lipase; Amano AK: *Pseudomonas fluorescens* lipase; Amano AYS; *Candida rugosa* lipase. [d]Absolute configurations were determined using their circular dichroism spectra. [e]50 mg of lipase was used at 20 °C.

were converted readily into **9** by treatment with 1 M NaOH (Figure S3 and Scheme 3). Helicene catechol would be air-

Scheme 3. Optical Resolution of 2 by Amano PS IM

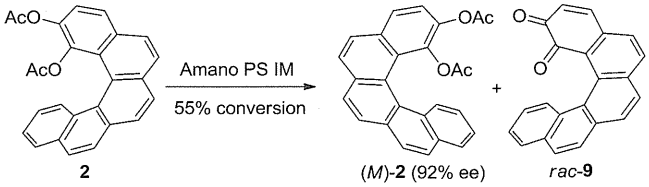

sensitive and undergo oxidation to give corresponding **9**.[6] Helicene **3a** is recovered with 92% *ee* at 55% conversion, while a solution of isolated **9** exhibited no optical activity due to the low racemization barrier (ΔG = 19.4 kcal mol^{-1} by DFT).[11]

The configurationally stable acetate *rac*-**3a** was not hydrolyzed at all by lipases. This may be due to the steric hindrance caused by the bulky helicene scaffold. Next, *rac*-**3a** was resolved to each enantiomer by using (1*S*)-10-camphorsulfonyl chloride as a resolving agent.[12] Treatment of *rac*-**3a** with (1*S*)-10-camphorsulfonyl chloride and Et_3N in CH_2Cl_2 at room temperature led to a mixture of two diastereomeric helicene camphorsulfonates, (*M*,*S*)-**10** and (*P*,*S*)-**10**, in 87% combined yield (Scheme 4). The diastereomers were separated on a silica gel column to give (*M*,*S*)-**10** (43%) and (*P*,*S*)-**10** (44%). The subsequent desulfonylation generated enantiomerically pure (*M*)-**3b** and (*P*)-**3b**. The relative configurations of diaster-

Scheme 4. Enantiomeric Resolution of 3b with (1*S*)-10-Camphorsulfonyl Chloride

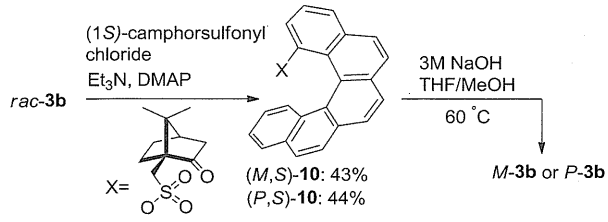

eomers (*M*,*S*)-**10** and (*P*,*S*)-**10** were confirmed by X-ray crystallography (Figure 3).

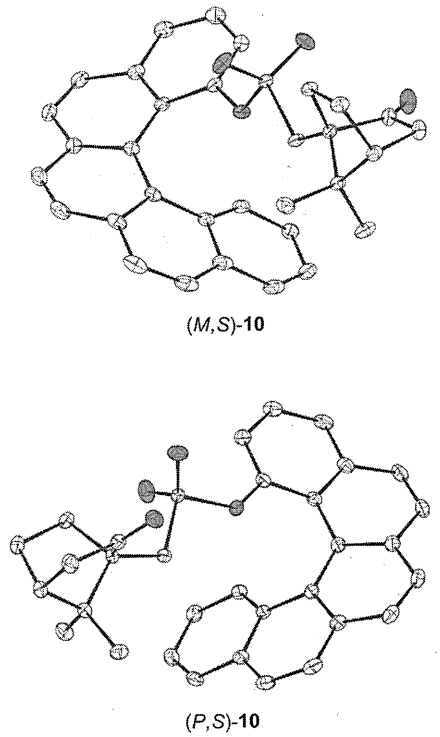

Figure 3. ORTEP drawing of (*M*,*S*)-10 and (*P*,*S*)-10 with 50% ellipsoid probability.

Next, we performed Amano PS lipase (PDB code 1YS1) docking studies in silico using transition state analogues ((*P*)-**1′** and (*P*)-**2′**) to understand the interactions between these molecules and lipase (Figure 4). The docking calculations were performed using *MacroModel*, and it was predicted that the phosphine oxide[13] (*P*)-intermediate forms hydrogen bonds with three amino acid residues, His286, Gln88, and Leu17, which stabilize the tetrahedral intermediate. It is noteworthy that in both intermediates the significant intramolecular H-bond interactions of the lipase are not interrupted.

In summary, after developing the synthesis of racemic [5]helicenyl acetates (**1a**–**3a**), we demonstrated their lipase-catalyzed kinetic resolution. The reactivity of [5]helicene toward enzymatic hydrolysis was found to be highly dependent on the position of the acetate group, as the enzymatic hydrolysis of substrate **3a** did not occur. We expect that this optical resolution protocol will prove to be useful in the synthesis of chiral [5]helicene compounds.

EXPERIMENTAL SECTION

General Information. All reagents and solvents were purchased from commercial sources and were used as received unless otherwise noted. Reagent grade solvents (CH_2Cl_2, toluene, DMSO, DMF) were distilled prior to use. Reactions were monitored by TLC (silica gel 60 F_{254}, 0.25 mm) analysis. Flash column chromatography was performed on flash silica gel 60N (spherical neutral, particle size 40–50 μm). HPLC analyses were conducted with a UV detector and a chiral column: Daicel Chiralpak IA (4.6 mm × 250 mm). ^1H and ^{13}C NMR were recorded in $CDCl_3$ as solvent at ambient temperature on a 400 or 500 MHz NMR spectrometer (100

DOI: 10.1021/acs.joc.5b00759
J. Org. Chem. 2015, 80, 6502–6508

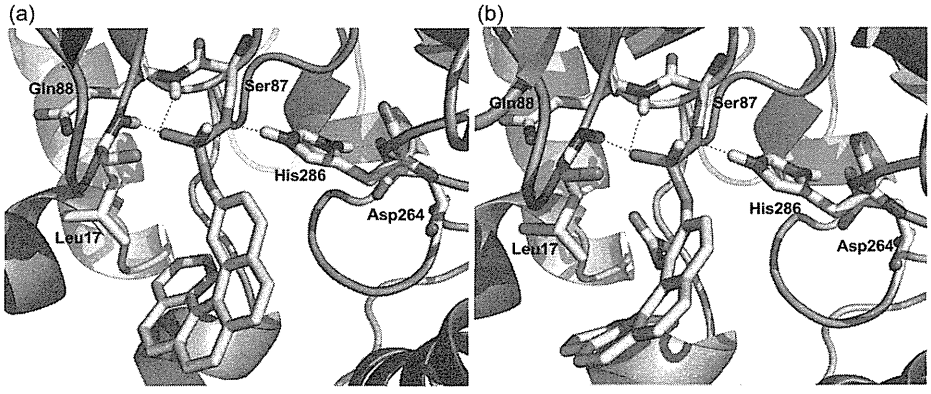

Figure 4. Modeled complexes of Amano PS with transition state analogue ((*P*)-**1′** (a) and (*P*)-**2′** (b)) showing the front view of the active site.

or 125 MHz for ^{13}C NMR). Chemical shifts were reported in parts per million (ppm) relative to internal tetramethylsilane (δ 0.00 ppm) or $CDCl_3$ (δ 7.26 ppm) for ^1H NMR and $CDCl_3$ (δ 77.0 ppm) for ^{13}C NMR. Coupling constants were reported as J values in Hertz (Hz). Splitting patterns are designated as s (singlet), d (doublet), t (triplet), dd (double of doublet), ddd (doublet of doublet of doublets), br (broad), and m (multiplet). Infrared spectra of neat samples were recorded in ATR (attenuated total reflectance) mode using an FT-IR instrument. HRMS were recorded on a ESI-TOF spectrometer. Optical rotations were measured with a polarimeter using a 0.5 dm cell. CD measurements were performed on a spectropolarimeter with an optical path length of 1.0 mm.

Dibenzo[*c,g*]phenanthren-9-yl acetate (1a). To a stirred solution of **1b** (0.20 g, 0.68 mmol) in CH_2Cl_2 (20 mL) at 0 °C under an argon atmosphere were added triethylamine (0.47 mL, 3.34 mmol) and acetic anhydride (0.13 mL, 1.36 mmol). The reaction mixture was allowed to warm to room temperature and stirred for 2 h. The reaction was quenched with water at 0 °C. The aqueous layer was extracted with CH_2Cl_2. The organic layers were combined, washed with water and brine, dried over $MgSO_4$, filtered, and concentrated under reduced pressure. The residue was purified by flash column chromatography on silica gel eluting with hexane-EtOAc (9:1) to afford **1a** (0.23 mg, quant.) as a pale yellow solid. (*P*)-(+)-**1a** $[\alpha]_D^{20}$ = +1860 (c 8.2 × 10^{-3}, $CHCl_3$), (*M*)-(−)-**1a** $[\alpha]_D^{20}$ = −1860 (c 8.2 × 10^{-3}, $CHCl_3$); mp =166–167 °C; IR (neat, cm^{-1}) 1758, 1368, 1206, 1170, 1033, 915, 848, 763, 747, 672, 663; UV–vis ($CHCl_3$): λ_{max} (log ε) = 332 (4.16), 305 (4.43), 269 (4.51), 240 (4.44) nm; ^1H NMR (500 MHz, $CDCl_3$): δ 8.55 (d, J = 8.5 Hz, 1H), 8.19 (d, J = 1.0 Hz, 1H), 7.95–7.83 (m, 8H), 7.51 (ddd, J = 8.0, 6.9, 1.1 Hz 1H), 7.32 (ddd, J = 8.4, 6.9, 1.4 Hz, 1H), 7.25 (dd, J = 8.7, 2.3 Hz, 1H), 2.20 (s, 3H); ^{13}C NMR (125 MHz, $CDCl_3$): δ 169.7, 147.5, 132.7, 132.6, 132.3, 131.6, 130.7, 130.3, 129.2, 128.9, 127.8, 127.7, 127.6, 127.2, 127.1, 127.0, 126.7, 126.4, 126.3, 124.9, 121.2, 120.7, 21.1; HRMS (ESI, Pos) m/z: $[M + Na]^+$ calcd for $C_{24}H_{16}O_2Na$ 359.1043, found 359.1075.

Dibenzo[*c,g*]phenanthren-9-ol (1b). To a solution of **1c** (0.97 g, 3.15 mmol) in CH_2Cl_2 (31 mL) at −10 °C under an argon atmosphere was added dropwise a 1.0 M solution of BBr_3 in CH_2Cl_2 (6.3 mL, 6.30 mmol). The reaction mixture was allowed to warm to room temperature and stirred for 3 h. The reaction was quenched with water at 0 °C. The aqueous layer was extracted and with CH_2Cl_2. The organic layers were combined, washed with water and brine, dried over $MgSO_4$, filtered, and concentrated under reduced pressure. The residue was purified by flash column chromatography on silica gel eluting with hexane–EtOAc (8:1) to afford **1b** (0.92 g, quant.) as a pale yellow solid. (*P*)-(+)-**1b** $[\alpha]_D^{20}$ = +2642 (c 2.1 × 10^{-2}, $CHCl_3$), (*M*)-(−)-**1b** $[\alpha]_D^{20}$ = −2811 (c 2.0 × 10^{-2}, $CHCl_3$); mp =188–191 °C; IR (neat, cm^{-1}) 3500, 2969, 1438, 1056, 1033, 1011, 873, 841, 829, 764, 714, 697; UV–vis ($CHCl_3$): λ_{max} (log ε) = 337 (4.21), 305 (4.36), 271 (4.45), 241 (4.50) nm; ^1H NMR (400 MHz, $CDCl_3$): δ 8.55 (d, J = 8.6 Hz,1H), 7.96–7.85 (m, 8H), 7.74 (d, J = 8.4 Hz, 1H), 7.52 (t, J = 7.2 Hz, 1H), 7.31 (t, J = 7.4 Hz, 1H), 7.13 (dd, J = 8.8, 2.5 Hz, 1H), 4.93 (s, 1H); ^{13}C NMR (100 MHz, $CDCl_3$,): δ 152.6, 132.8, 132.7, 132.1, 132.1, 130.3, 129.7, 129.3, 127.6, 127.3, 127.3, 127.1, 126.5, 126.1, 125.9, 124.2, 124.1, 112.5; HRMS (ESI, Pos) m/z: $[M + Na]^+$ calcd for $C_{22}H_{14}NaO$ 317.0937, found 317.0944.

9-Methoxydibenzo[*c,g*]phenanthrene (1c). A solution of **8** (3.45 g, 11.18 mmol) and $PtCl_2$ (0.15 g, 5 mol %) in toluene (56 mL) was stirred at 85 °C for 8 h under an argon atmosphere. After cooling to room temperature, the solvent was evaporated and the residue was purified by flash column chromatography on silica gel eluting with hexane–EtOAc (95:5) to afford **1c** (2.58 g, 75%) as a pale yellow solid. (*P*)-(+)-**1c** $[\alpha]_D^{20}$ = +2463 (c 4.5 × 10^{-2}, $CHCl_3$), (*M*)-(−)-**1c** $[\alpha]_D^{20}$ = −2258 (c 1.6 × 10^{-3}, $CHCl_3$); mp =144–145 °C; IR (neat, cm^{-1}) 2966, 1231, 1054, 1033, 1011, 873, 842, 747; UV–vis ($CHCl_3$): λ_{max} (log ε) = 401 (2.81), 381 (3.63), 304 (4.41), 270 (4.48), 242 (4.53) nm; ^1H NMR (400 MHz, $CDCl_3$): δ 8.46 (d, J = 8.6 Hz,1H), 7.97–7.84 (m, 8H), 7.77 (d, J = 8.4 Hz, 1H), 7.51 (t, J = 7.1 Hz, 1H), 7.33 (t, J = 7.7 Hz, 1H), 7.17 (dd, J = 8.8, 2.6 Hz, 1H), 3.49 (s, 3H); ^{13}C NMR (100 MHz, $CDCl_3$): δ 156.5, 132.7, 132.6, 132.1, 131.9, 130.2, 129.7, 129.3, 127.9, 127.6, 127.4, 127.2, 127.1, 127.0, 126.4, 126.2, 126.1, 124.1, 124.0, 118.0, 109.2, 54.8; HRMS (ESI, Pos) m/z: $[M + Na]^+$ calcd for $C_{23}H_{16}NaO$ 331.1093, found 331.1093.

2-Bromo-12-methoxydibenzo[*c,g*]phenanthrene (1d). Compound **1d** was prepared according to Majetich's procedure.[14] To a solution of **1c** (30.0 mg, 0.10 mmol) in acetic acid (0.6 mL) were added dropwise 48% aqueous HBr (0.9 mL) and DMSO (0.8 mL). The reaction mixture was stirred at room temperature for 44 h. After cooling to 0 °C, the reaction mixture was treated with saturated aqueous solution of $NaHCO_3$ to adjust to pH = 6 and then extracted with EtOAc, dried over $MgSO_4$, filtered, and concentrated under reduced pressure. The residue was purified by flash column chromatography on silica gel eluting with hexane-CH_2Cl_2 (9:1) to afford **1d** (10.0 mg, 26%) as a yellow solid. mp = 204–206 °C; IR

DOI: 10.1021/acs.joc.5b00759
J. Org. Chem. 2015, 80, 6502–6508

(neat, cm^{-1}) 2938, 1231, 1056, 1033, 1012, 880, 840, 806, 753; ^1H NMR (400 MHz, $CDCl_3$): δ 8.36 (t, J = 8.6 Hz, 2H), 8,20, (s, 1H), 7.96–7.87 (m, 4H), 7.77–7.74 (m, 2H), 7.53–7.50 (m, 1H), 7.34–7.30 (m, 1H), 7.18 (dd, J = 8.8, 2.4 Hz, 1H), 3.45 (s, 3H); ^{13}C NMR (100 MHz, $CDCl_3$): δ 157.4, 133.2, 133.8, 131.7, 131.3, 130.7, 130.6, 130.0, 128.9, 128.4, 128.3, 1278.0, 127.0, 126.8, 126.6, 126.4, 124.9, 119.0, 118.6, 110.7, 55.2; HRMS (ESI, Pos) m/z: $[M + Na]^+$ calcd for $C_{23}H_{15}BrNaO$ 409.0198, found 409.0204.

Dibenzo[*c,g*]phenanthrene-9,10-diyl Diacetate (2). (a) To a solution of **1b** (30.0 mg, 0.10 mmol) in DMF (0.8 mL) at 0 °C under an argon atmosphere was added 81 mg (0.11 mmol) of stabilized 2-iodoxybenzoic acid (IBX) composition (39% w/w of IBX). The mixture was allowed to warm to room temperature and stirred for 1 h. The reaction mixture was diluted with hexane–EtOAc (4:1), and the organic layers were washed with water and with brine. The organic layers was dried over Na_2SO_4, filtered, and concentrated under reduced pressure to give the crude product as a dark red solid. The crude mixture was dried in vacuo for 1 h, and then subjected to the next reaction without further purification. (b) To a crude solution of **9** in DMF (0.5 mL) at 0 °C under an argon atmosphere was added $NaBH_4$ (19 mg, 0.50 mmol). The mixture was allowed to warm to room temperature and stirred for 0.5 h. To the reaction mixture were added acetic anhydride (57 μL, 0.60 mmol) and Na_2CO_3 (64 mg, 0.60 mmol). After 20 h, additional acetic anhydride (57 μL, 0.6 mmol) was added and the mixture was stirred overnight. The reaction was quenched with water at 0 °C. The aqueous layer was extracted and with hexane–EtOAc (4:1). The organic layers were combined, washed with water and brine, dried over anhydrous Na_2SO_4, filtered, and concentrated under reduced pressure. The residue was purified by flash column chromatography on silica gel eluting with hexane–Et_2O (8:1) to give **2** (27.0 mg, 68%) as an ivory solid. (*P*)-(+)-**2** $[\alpha]_D^{20}$ = +1702 (c 11.3 × 10^{-3}, $CHCl_3$), (*M*)-(−)-**2** $[\alpha]_D^{20}$ = −1665 (c 13.3 × 10^{-3}, $CHCl_3$); mp = 213–215 °C; IR (neat, cm^{-1}); 3276, 2969, 2331, 1764, 1371, 1205, 1159, 1057, 1033, 1012, 841, 746, 675, 659; UV–vis ($CHCl_3$): λ_{max} (log ε) = 309 (4.57), 266 (4.43), 240 (4.49) nm; ^1H NMR (500 MHz, $CDCl_3$): δ 8.21 (d, J = 8.5 Hz, 1H), 7.91–7.77 (m, 8H), 7.50 (ddd, J = 8.0, 7.0, 1.0 Hz 1H), 7.41 (d, J = 8.5 Hz, 1H), 7.31 (ddd, J = 8.0, 7.0, 1.0 Hz, 1H), 2.18 (s, 3H), 1.03 (s, 3H); ^{13}C NMR (125 MHz, $CDCl_3$): δ 168.8, 167.01, 140.8, 139.0, 133.2, 132.6, 132.1, 131.3, 131.0, 128.3, 127.6, 127.4, 127.3, 127.0, 126.9, 126.7, 126.4, 126.1, 126.0, 125.7, 122.3, 121.7, 20.7, 19.3; HRMS (ESI, Pos) m/z: $[M + Na]^+$ calcd for $C_{26}H_{18}O_4Na$ 417.1097, found 417.1135.

Dibenzo[*c,g*]phenanthren-10-yl Acetate (3a). To a stirred solution of **3b** (50.0 mg, 0.17 mmol) in CH_2Cl_2 (1.7 mL) at 0 °C under an argon atmosphere were added triethylamine (36.0 μL, 0.25 mmol) and acetic anhydride (24.0 μL, 0.25 mmol). The mixture was allowed to warm to room temperature and stirred for 1.5 h. The reaction was quenched with water at 0 °C. The aqueous layer was extracted and with EtOAc. The organic layers were combined, washed with water and brine, dried over anhydrous Na_2SO_4, filtered, and concentrated under reduced pressure. The residue was purified by flash column chromatography on silica gel eluting with hexane–Et_2O (5:1) to give **3a** (49.0 mg, 98%) as a white solid. (*P*)-(+)-**3a** $[\alpha]_D^{20}$ = +2046 (c 1.3 × 10^{-2}, $CHCl_3$), (*M*)-(−)-**3a** $[\alpha]_D^{20}$ = −1815 (c 1.3 × 10^{-2}, $CHCl_3$); mp = 155–1157 °C; IR (neat, cm^{-1}) 3462, 2328, 1755, 1203, 838, 751, 671, 659; UV–vis ($CHCl_3$): λ_{max} (log ε) = 309 (4.55), 266 (4.42), 240 (4.41), 270 (4.45) nm; ^1H NMR (500 MHz, $CDCl_3$): δ 8.14 (d, J = 8.5 Hz, 1H), 7.94–7.85 (m, 8H), 7.60 (t, J = 7.8 Hz, 1H), 7.52 (ddd, J = 8.0, 6.9, 1.1 Hz, 1H), 7.26 (ddd, J = 7.8, 6.9, 1.4 Hz, 1H), 7.17 (dd, J = 8.7, 1.1 Hz, 1H), 1.03 (s, 3H); ^{13}C NMR (125 MHz, $CDCl_3$): δ 168.1, 147.9, 134.4, 132.9, 132.8, 131.2, 131.1, 127.9, 127.7, 127.5, 127.1, 127.0, 126.7, 126.3, 125.9, 125.8, 125.7, 125.4, 124.8, 122.3, 119.4, 19.7; HRMS (ESI, Pos) m/z: $[M + Na]^+$ calcd for $C_{24}H_{16}O_2Na$ 359.1043, found 359.1062.

Dibenzo[*c,g*]phenanthren-10-ol ((*M*)-(−)-3b and (*P*)-(+)-3b). To a solution of **10** (25.0 mg, 0.05 mmol, dr 20:1) in 2 mL of THF/MeOH (3:1) was added 3 M NaOH (0.5 mL). The reaction mixture was heated at 60 °C for 1 h. After cooling to room temperature, the reaction mixture was neutralized with 10% HCl and extracted with Et_2O. The organic layers were combined; washed with saturated aqueous $NaHCO_3$, water, and brine; dried over $MgSO_4$; filtered; and concentrated under reduced pressure. The residue was purified by flash column chromatography on silica gel eluting with hexane–EtOAc (9:1) to give **3b**. (*M*)-(−)-**3b** (12.9 mg, 88%, 93% *ee*) was obtained from (*M,S*)-**10** as a pale yellow foam. (*P*)-(+)-**3b** (13.4 mg, 91%, 91% *ee*) was obtained from (*P,S*)-**10** as a pale yellow foam. (*M*)-(−)-**3b**: ^1H NMR (500 MHz, $CDCl_3$): δ 8.27 (d, J = 8.6 Hz,1H), 8.00–7.93 (m, 6H), 7.85 (d, J = 8.5 Hz, 1H), 7.65 (d, J = 7.8 Hz, 1H), 7.59–7.55 (m, 2H), 7.31 (ddd, J = 8.4, 7.1, 1.3 Hz, 1H), 6.95 (dd, J = 7.6, 1.0 Hz, 1H), 5.11 (br s, 1H). (*P*)-(−)-**3b**: ^1H NMR (500 MHz, $CDCl_3$): δ 8.27 (d, J = 8.6 Hz,1H), 8.00–7.93 (m, 6H), 7.85 (d, J = 8.5 Hz, 1H), 7.65 (d, J = 7.9 Hz, 1H), 7.59–7.55 (m, 2H), 7.31 (t, J = 7.6 Hz, 1H), 6.95 (d, J = 7.6 Hz, 1H), 5.11 (br s, 1H). Spectroscopic data are consistent with our previous report.[1a]

1-Chloro-7-methoxy-3,4-dihydronaphthalene-2-carbaldehyde (5). To a solution of DMF (4.4 mL, 56.70 mmol) at 0 °C was added dropwise $POCl_3$ (4.2 mL, 45.40 mmol). The reaction mixture was warmed to 90 °C and stirred for 1 h to form the Vilsmeier salt. After cooling to 0 °C, 7-methoxy-α-tetralone (**4**) (5.0 g, 28.40 mmol) was added, and the reaction mixture was stirred at 90 °C for 2 h. The reaction was quenched with saturated aqueous $NaHCO_3$ at 0 °C. The aqueous layer was extracted and with CH_2Cl_2. The organic layers were combined, washed with water and brine, dried over anhydrous Na_2SO_4, filtered, and concentrated under reduced pressure. The residue was purified by flash column chromatography on silica gel eluting with hexane–EtOAc (9:1) to afford **5** (5.7 g, 91%) as an orange solid. ^1H NMR (400 MHz, $CDCl_3$): δ 10.39 (s, 1H), 7.42 (d, J = 2.6 Hz, 1H), 7.14 (d, J = 8.2 Hz, 1H), 6.92 (dd, J = 8.2, 2.6 Hz, 1H), 3.86 (s, 3H), 2.80–2.76 (m, 2H), 2.65–2.60 (m, 2H). Spectroscopic data are consistent with the literature.[15]

7-Methoxy-3,4-dihydro-[1,1′-binaphthalene]-2-carbaldehyde (6). A suspension of **5** (690 mg, 3.1 mmol), 1-naphtylboronic acid (0.58 g, 3.40 mmol), tetrabutylammonium bromide (0.99 g, 3.10 mmol), $Pd(OAc)_2$ (34.0 mg, 5 mol %), and K_2CO_3 (0.85 g, 6.10 mmol) in degassed water (6 mL) was stirred at 45 °C under an argon atmosphere for 1.5 h. After cooling to room temperature, the reaction mixture was diluted with water and extracted with EtOAc. The organic layers were combined, washed with water and brine, dried over $MgSO_4$, filtered, and concentrated under reduced pressure. The residue was purified by flash column chromatography on silica gel eluting with hexane–EtOAc (9:1) to afford **6** (0.97 g, quant.) as a pale yellow solid. mp = 100–103 °C; IR (neat, cm^{-1}) 2928, 1655, 1566, 1362, 1300, 1232, 1124, 1044, 815, 798, 779, 747,

DOI: 10.1021/acs.joc.5b00759
J. Org. Chem. 2015, 80, 6502–6508

709; ^{1}H NMR (400 MHz, $CDCl_3$): δ 9.38 (s, 1H), 7.92 (dd, J = 12.5, 8.2 Hz, 2H), 7.58–7.46 (m, 3H), 7.42–7.36 (m, 2H), 7.22 (d, J = 8.2 Hz, 1H), 6.81 (dd, J = 8.2, 2.6 Hz, 1H), 6.21 (d, J = 2.6 Hz, 1H), 3.21 (s, 3H), 3.00–2.83 (m, 3H), 2.73–2.64 (m, 1H); ^{13}C NMR (100 MHz, $CDCl_3$): δ 193.0, 158.3, 152.9, 136.3, 136.1, 133.5, 132.7, 132.6, 130.3, 128.9, 128.5, 128.4, 126.8, 126.3, 125.8, 125.0, 114.8, 114.4, 55.1, 26.8, 20.5; HRMS (ESI, Pos) m/z: $[M + Na]^+$ calcd for $C_{22}H_{18}NaO_2$ 337.1199, found 337.1195.

7-Methoxy-[1,1′-binaphthalene]-2-carbaldehyde (7). To a stirred solution of **6** (1.44 g, 4.60 mmol) in toluene (26 mL) was added DDQ (1.40 g, 5.7 mmol). The resulting solution was heated at 60 °C for 3 h. After cooling to room temperature, the resultant precipitate was removed by suction filtration. The filtrate was washed with 1 N NaOH and extracted with toluene. The organic layers were combined, washed with water and brine, dried over $MgSO_4$, filtered, and concentrated under reduced pressure. The residue was purified by flash column chromatography on silica gel eluting with hexane–EtOAc (9:1) to afford **7** (1.43 g, quant.) as a white solid. mp = 75–76 °C; IR (neat, cm^{-1}) 3007, 1688, 1620, 1506, 1454, 1425, 1275, 1178, 1070, 1027, 983, 843, 808, 790, 778, 730; ^{1}H NMR (400 MHz, $CDCl_3$): δ 9.64 (s, 1H), 8.04–7.94 (m, 4H), 7.87 (d, J = 9.0 Hz, 1H), 7.63 (t, J = 7.7 Hz, 1H), 7.53–7.48 (m, 2H), 7.32 (m, 1H), 7.28–7.23 (m,2H), 6.63 (d, J = 7.7 Hz, 1H), 3.49 (s, 3H); ^{13}C NMR (100 MHz, $CDCl_3$): δ 192.5, 158.2, 143.3, 134.3, 133.3, 133.2, 133.1, 132.5, 131.6, 129.6, 129.0, 128.8, 128.3, 126.7, 126.2, 126.0, 125.0, 121.0, 120.0, 106.2, 55.0; HRMS (ESI, Pos) m/z: $[M + Na]^+$ calcd for $C_{22}H_{16}NaO_2$ 335.1043, found 335.1043.

2-Ethynyl-7-methoxy-1,1′-binaphthalene (8). To a stirred suspension of **7** (3.75 g, 12.0 mmol) and K_3PO_4 (3.31 g, 15.6 mmol) in MeOH (120 mL) at room temperature under an argon atmosphere was added a solution of Ohira-Bestmann reagent (3.43 g, 15.6 mmol) in MeOH (15.6 mL). The reaction mixture was stirred overnight at the same temperature. After removing the MeOH under reduced pressure, the residue was diluted with EtOAc and washed with H_2O. The organic layers were combined, washed with water and brine, dried over $MgSO_4$, filtered, and concentrated under reduced pressure. The residue was purified by flash column chromatography on silica gel eluting with hexane–EtOAc (95:5) to afford **8** (3.45 g, 93%) as a pale yellow solid. mp = 87–89 °C; IR (neat, cm^{-1}) 3285, 2970, 1619, 1506, 1458, 1419, 1274, 1258, 1144, 1056, 1033, 844, 781; ^{1}H NMR (400 MHz, $CDCl_3$): δ 7.95 (t, J = 8.8 Hz, 2H), 7.82 (dd, J = 8.7, 6.5 Hz, 2H), 7.70–7.75 (m, 2H), 7.49–7.45 (m, 2H), 7.30–7.29 (m, 2H), 7.15 (dd, J = 9.0, 2.6 Hz, 1H), 6.51 (d, J = 2.4 Hz, 1H), 3.47 (s, 3H), 2.77 (s, 1H); ^{13}C NMR (100 MHz, $CDCl_3$): δ 158.1, 140.7, 136.6, 134.0, 133.6, 132.4, 129.4, 128.7, 128.1, 128.1, 128.0, 127.5, 126.8, 126.1, 126.0, 126.0, 125.4, 120.6, 119.0, 105.5, 83.3, 80.8, 55.0; HRMS (ESI, Pos) m/z: $[M + Na]^+$ calcd for $C_{23}H_{16}NaO$ 331.1093, found 331.1105.

Dibenzo[*c*,*g*]phenanthrene-9,10-dione (9). To a solution of **1b** (30 mg, 0.10 mmol) in DMF (mL) at 0 °C under an argon atmosphere was added 81 mg (0.11 mmol) of stabilized 2-iodoxybenzoic acid (IBX) composition (39% w/w of IBX). The reaction mixture was allowed to warm to room temperature and stirred for 1 h. The reaction mixture was extracted with EtOAc, washed with water, dried over anhydrous Na_2SO_4, filtered, and concentrated under reduced pressure to give the crude product. The crude product was purified by flash column chromatography over silica gel with hexane–Et_2O (1:1) to give the compound **9** as a dark red solid (30 mg, 97% yield). mp = 166 °C (decomposition); IR (neat, cm^{-1}) 2923, 2330, 1733, 1389, 1262, 1055, 1033, 1013, 808, 759, 724, 689, 656; UV–vis ($CHCl_3$): λ_{max} (log ε) = 368 (3.42), 351 (3.39), 298 (4.06), 280 (4.07), 243 (4.23) nm; ^{1}H NMR (500 MHz, $CDCl_3$): δ 8.41 (d, J = 8.0 Hz, 1H), 8.13 (d, J = 8.0 Hz, 1H) 7.97–7.78 (m, 5H), 7.65 (d, J = 9.6 Hz, 1H), 7.54–7.47 (m, 3H), 6.49 (d, J = 10.0 Hz, 1H); ^{13}C NMR (125 MHz, $CDCl_3$): δ 185.0, 184.4, 146.8, 136.3, 135.9, 135.7, 134.8, 133.3, 133.3, 131.8, 130.0, 128.8, 128.7, 128.6, 128.5, 127.8, 127.6, 127.1, 127.0, 126.6, 126.3; HRMS (ESI, Pos) m/z: $[M + Na]^+$ calcd for $C_{22}H_{12}O_2Na$ 331.0730, found 331.0744.

Dibenzo[*c*,*g*]phenanthren-10-yl ((1*S*)-7,7-dimethyl-2-oxobicyclo[2.2.1]heptan-1-yl)methanesulfonate ((*M*,*S*)-10 and (*P*,*S*)-10). To a stirred solution of *rac*-3b (48.0 mg, 0.16 mmol) and (1*S*)-camphorsulfonyl chloride (0.10 g, 0.40 mmol) in CH_2Cl_2 at 0 °C under an argon atmosphere were added triethylamine (81.0 mg, 0.80 mmol) and DMAP (2.4 mg, 0.02 mmol). The reaction mixture was allowed to warm to room temperature and stirred for 15 min. The reaction was quenched with 10% HCl. The resultant solution was neutralized with saturated aqueous $NaHCO_3$ and extracted with CH_2Cl_2. The organic layers were combined, washed with water and brine, dried over $MgSO_4$, filtered, and concentrated under reduced pressure. The diastereomixture was separated by flash column chromatography on silica gel eluting with hexane-Et_2O-EtOAc (8:1:1) to afford (*M*,*S*)-**10** (early eluting fraction) as a white foam (35.0 mg, 43%, dr 20:1) and (*P*,*S*)-**10** (late eluting fraction) as white foam (36.0 mg, 44%, dr 20:1). (*M*,*S*)-**10**: $[\alpha]_D^{20}$ = −1350 (c 4.0 × 10^{-3}, $CHCl_3$); mp = 222–225 °C; IR (neat, cm^{-1}) 1747, 1354, 1177, 1160, 1101, 1055, 996, 913, 843, 824, 674, 684; UV–vis ($CHCl_3$): λ_{max} (log ε) = 310 (4.51), 266 (4.40), 240 (4.40) nm; ^{1}H NMR (500 MHz, $CDCl_3$): δ 8.06 (d, J = 8.5 Hz, 1H), 8.00–7.86 (m, 8H), 7.62 (t, J = 7.8 Hz, 1H), 7.54 (ddd, J = 8.0, 6.9, 1.1 Hz, 1H), 7.46 (dd, J = 7.6, 1.2 Hz, 1H), 7.28 (ddd, J = 8.5, 6.4, 1.4 Hz, 1H), 2.48 (d, J = 14.8 Hz, 1H), 2.24 (ddd, J = 16.9, 3.8, 3.8 Hz, 1H), 1.93–1.88 (m, 2H), 1.81–1.73 (m, 2H), 1.32 (d, J = 14.8 Hz, 1H), 1.29–1.19 (m, 2H), 0.67 (s, 3H), 0.59 (s, 3H); ^{13}C NMR (125 MHz, $CDCl_3$): δ 213.1, 144.8, 134.7, 133.1, 132.6, 131.3, 131.1, 128.2, 128.1, 127.9, 127.8, 127.4, 126.94, 126.90, 126.7, 126.6, 126.3, 125.7, 125.6, 125.5, 125.4, 122.1, 120.9, 57.2, 47.6, 47.1, 42.6, 42.3, 26.7, 24.3, 19.4, 19.3; HRMS (ESI, Pos) m/z: $[M + Na]^+$ calcd for $C_{32}H_{28}NaO_4S$ 531.1601, found 531.1605. (*P*,*S*)-**10**: $[\alpha]_D^{20}$ = +1100 (c 4.0 × 10^{-3}, $CHCl_3$); mp = 185–188 °C; IR (neat, cm^{-1}) 1747, 1357, 996, 913, 842, 675, 663; UV–vis ($CHCl_3$): λ_{max} (log ε) = 310 (4.55), 266 (4.43), 240 (4.42) nm; ^{1}H NMR (500 MHz, $CDCl_3$): δ 8.07 (d, J = 8.6 Hz, 1H), 8.02–7.87 (m, 8H), 7.62 (t, J = 7.8 Hz, 1H), 7.53 (ddd, J = 8.0, 6.9, 1.1 Hz, 1H), 7.42 (dd, J = 7.7, 1.3 Hz, 1H), 7.29–7.26 (m, 1H), 2.18 (ddd, J = 18.4, 4.7, 2.5 Hz, 1H), 2.00 (d, J = 14.8 Hz, 1H), 1.93–1.79 (m, 3H), 1.73 (s, 1H), 1.69 (d, J = 3.2 Hz, 1H), 1.25–1.22 (m, 2H), 0.78 (s, 3H), 0.58 (s, 3H); ^{13}C NMR (125 MHz, $CDCl_3$): δ 213.1, 145.5, 134.7, 133.1, 132.6, 131.4, 131.1, 128.3, 128.2, 127.8, 127.7, 127.4, 127.0, 126.9, 126.7, 126.40, 126.35, 125.6, 125.64, 125.58, 124.9, 121.9, 120.5, 57.3, 47.6, 46.9, 42.7, 42.2, 26.7, 24.7, 19.6, 19.4; HRMS (ESI, Pos) m/z: $[M + Na]^+$ calcd for $C_{32}H_{28}NaO_4S$ 531.1601, found 531.1606.

DOI: 10.1021/acs.joc.5b00759
J. Org. Chem. 2015, 80, 6502–6508

■ ASSOCIATED CONTENT

Supporting Information

^{1}H and ^{13}C NMR spectra of all new compounds, ORTEP/X-ray and CIF data for single-crystal X-ray analyses of compounds **1d** (CCDC 901873), (*M*, *S*)-**10** (CCDC 1051698), and (*P*, *S*)-**10** (CCDC 1051700), HPLC analysis graphs for enzymatic hydrolysis experiments for compounds **1a** and **2**, kinetic data for racemization for compounds **1a**–**c**, computational details, Cartesian coordinates for all calculated structures, ORTEP drawings of compounds **1d**, (*P*, *S*)-**10**, and (*M*, *S*)-**10**, CD spectra of **1a**, **1b**, **1c**, **2**, **3a**, and **10**. The Supporting Information is available free of charge on the ACS Publications website at DOI: 10.1021/acs.joc.5b00759.

■ AUTHOR INFORMATION

Corresponding Authors

*E-mail: usui@phar.kyushu-u.ac.jp.

*E-mail: suemune@phar.kyushu-u.ac.jp.

Notes

The authors declare no competing financial interest.

■ ACKNOWLEDGMENTS

This work was financially supported by a Grant-in-Aid for Scientific Research (C) from the Japan Society for the Promotion of Science (No. 25410096) and Platform for Drug Discovery, Informatics, and Structural Life Science from the Ministry of Education, Culture, Sports, Science and Technology, Japan. K.Y. acknowledges support from JSPS research fellowship. We thank Amano Pharmaceutical Co., Ltd., for kindly providing lipases. We also thank Professor Masakazu Tanaka (Nagasaki University) for the helpful discussions.

■ REFERENCES

(1) (a) Yamamoto, K.; Okazumi, M.; Suemune, H.; Usui, K. *Org. Lett.* **2013**, *15*, 1806. (b) Guin, J.; Bürgi, T.; Guénée, L.; Lacour, J. *Org. Lett.* **2014**, *16*, 3800. (c) Zhang, Y.; Petersen, J. L.; Wang, K. K. *Org. Lett.* **2007**, *9*, 1025. (d) Jančařík, A.; Rybáček, J.; Cocq, K.; Chocholoušová, J. V.; Vacek, J.; Pohl, R.; Bednárová, L.; Fiedler, P.; Císařová, I.; Stará, I. G.; Starý, I. *Angew. Chem., Int. Ed.* **2013**, *52*, 9970.

(2) For reviews, see: (a) Shen, Y.; Chen, C.–F. *Chem. Rev.* **2012**, *112*, 1463. (b) Gingras, M. *Chem. Soc. Rev.* **2013**, *42*, 968. (c) Gingras, M.; Félix, G.; Peresutti, R. *Chem. Soc. Rev.* **2013**, *42*, 1007. (d) Gingras, M. *Chem. Soc. Rev.* **2013**, *42*, 1051. (e) Peng, Z.; Takenaka, N. *Chem. Res.* **2013**, *13*, 28. (f) Aillard, P.; Voituriez, A.; Marinetti, A. *Dalton Trans.* **2014**, *43*, 15263.

(3) Tanaka, K.; Shogase, Y.; Osuga, H.; Suzuki, H.; Nakamura, K. *Tetrahedron Lett.* **1995**, *36*, 1675.

(4) Liu, L. B.; Katz, T. J. *Tetrahedron Lett.* **1990**, *31*, 3983.

(5) Some recent papers on the synthesis of [5]helicene derivatives starting from 7-methoxy-1-tetralone, see; (a) Chen, J.-D.; Lu, H.-Y.; Chen, C.-F. *Chem.—Eur. J.* **2010**, *16*, 11843. (b) Shen, Y.; Lu, H.-Y.; Chen, C.-F. *Angew. Chem., Int. Ed.* **2014**, *53*, 4648. (c) Li, M.; Niu, Y.; Zhu, X.; Peng, Q.; Lu, H.-Y.; Xia, A.; Chen, C.-F. *Chem. Commun.* **2014**, *50*, 2993. (d) Li, M.; Feng, L.-H.; Lu, H.-Y.; Wang, S.; Chen, C.-F. *Adv. Funct. Mater.* **2014**, *24*, 4405.

(6) *Ortho*-quinone helicene, see: Schweinfurth, D.; Zalibera, M.; Kathan, M.; Shen, C.; Mazzolini, M.; Trapp, N.; Crassous, J.; Gescheidt, G.; Diederich, F. *J. Am. Chem. Soc.* **2014**, *136*, 13045.

(7) Regioselective IBX oxidation, see: (a) Wu, A.; Duan, Y.; Xu, D.; Penning, T. M.; Harvey, R. G. *Tetrahedron* **2010**, *66*, 2111. (b) Pouységu, L.; Sylla, T.; Garnier, T.; Rojas, L. B.; Charris, J.; Deffieux, D.; Quideau, S. *Tetrahedron* **2010**, *66*, 5908. (c) Pezzella, A.; Lista, L.; Napolitano, A.; d'Ischia, M. *Tetrahedron Lett.* **2005**, *46*, 3541. (d) Magdziak, D.; Rodriguez, A. A.; Van De Water, R. W.; Pettus, T. R. R. *Org. Lett.* **2002**, *4*, 285. (e) Nicolaou, K. C.; Montagnon, T.; Baran, P. S.; Zhong, Y.-L. *J. Am. Chem. Soc.* **2002**, *124*, 2245.

(8) The regioselectivity of oxygen insertion for *rac*-**1b** did not change from that of the 2-naphotol and 3-phenanthrenol building blocks.

(9) The absolute configuration of [5]helicenes was established by the CD exciton chirality method (Figure S1).

(10) Gibbs's free energy barriers to racemization ($\Delta G^{\ddagger}$) of **1a** and **1b** were measured on the basis of the time-dependent conversion rate (% *ee*) estimated from chiral HPLC analysis (Figure S4). The $\Delta G^{\ddagger}$ value at 303 K of **1a** and **1b** were almost the same as that of [5]helicene.

(11) Gibb's free energy barriers to racemization ($\Delta G^{\ddagger}$) of **9** could not be determined because it decomposed. Hence, the racemization barrier of **9** is estimated by DFT (Figure S6).

(12) (a) Thongpanchang, T.; Paruch, K.; Katz, T. J.; Rheingold, A. L.; Lam, K.-C.; Liable-Sands, L. *J. Org. Chem.* **2000**, *65*, 1850. (b) Braiek, M. B.; Aloui, F.; Hassine, B. B. *Tetrahedron. Lett.* **2013**, *54*, 424. (c) Surampudi, S. K.; Nagarjuna, G.; Okamoto, D.; Chaudhuri, P. D.; Venkataraman, D. *J. Org. Chem.* **2012**, *77*, 2074.

(13) Tanaka, M.; Demizu, Y.; Nagano, M.; Hama, M.; Yoshida, Y.; Kurihara, M.; Suemune, H. *J. Org. Chem.* **2007**, *72*, 7750.

(14) Majetich, G.; Hicks, R.; Reister, S. *J. Org. Chem.* **1997**, *62*, 4321.

(15) LaFrate, A. L.; Gunther, J. R.; Carlson, K. E.; Katzenellenbogen, J. A. *Bioorg. Med. Chem.* **2008**, *16*, 10075.

DOI: 10.1021/acs.joc.5b00759
J. Org. Chem. 2015, 80, 6502–6508

Tetrahedron 71 (2015) 2241–2245

Contents lists available at ScienceDirect

Tetrahedron

journal homepage: www.elsevier.com/locate/tet

Synthesis of a bis-cationic α,α-disubstituted amino acid (9-amino-bispidine-9-carboxylic acid) and its effects on the conformational properties of peptides

Hiroko Yamashita [a,b], Yosuke Demizu [a,*], Takashi Misawa [a], Takuji Shoda [a], Masaaki Kurihara [a,b,*]

[a] Division of Organic Chemistry, National Institute of Health Sciences, 1-18-1, Kamiyoga, Setagaya, Tokyo 158-8501, Japan
[b] Graduate School of Bioscience and Biotechnology, Tokyo Institute of Technology, Yokohama 226-8501, Japan

ARTICLE INFO

Article history:
Received 2 February 2015
Received in revised form 19 February 2015
Accepted 21 February 2015
Available online 26 February 2015

Keywords:
Cationic amino acid
α,α-disubstituted amino acid
Peptide
Conformational analysis

ABSTRACT

A new bis-cationic cyclic amino acid, 9-amino-3,7-diazabicyclo[3.3.1]nonane-9-carboxylic acid (9-amino-bispidine-9-carboxylic acid; Abp), which is available for both solution phase and solid phase peptide synthesis, was designed and synthesized. Furthermore, a heterotripeptide Cbz-Leu-Abp-Ala-OMe (**9**) containing Abp was prepared, and its dominant conformation was analyzed by examining its nuclear magnetic resonance and infrared spectra and performing molecular modeling. The tripeptide **9** formed a β-turn structure as its preferred conformation in solution.

1. Introduction

Naturally basic (cationic) amino acids, e.g., arginine, histidine, and lysine, in proteins and peptides play important roles in biological and chemical activities. Cationic peptides have unique properties, e.g., they can exhibit cell-penetrating and antimicrobial activity.[1] The stabilization of peptides' secondary structures, particularly their helical structures, has been demonstrated to be effective at enhancing their biological activities.[2] Non-proteinogenic amino acids, such as α,α-disubstituted α-amino acids (dAA)[3] and cyclic β-amino acids,[4] are often utilized as tools for peptide-helix stabilization. dAA, in which the α-hydrogen atoms of α-amino acids are replaced with alkyl substituents, are often incorporated into biologically active peptides to stabilize their helical structures or fully extended conformations,[5] and peptides containing dAA are also more resistant to proteolytic degradation.[6] To date, several cationic acyclic and cyclic dAA have been synthesized, and the conformations and properties of peptides containing these residues have been studied. Among cationic cyclic dAA, 4-aminopiperidine-4-carboxylic acid (Api),[7] which contains a piperidine ring, has been commonly used as a mimic of naturally occurring cationic amino acids, such as lysine and arginine, and is also used as a helical promoter in antimicrobial peptides. On the other hand, the bis-cationic acyclic amino acid bis-ornithine [bis(Orn)] causes peptides to adopt fully extended conformations,[8] and [bis(Orn)] oligopeptides are also used for cargo delivery.[9] Thus, these non-proteinogenic cationic amino acids are widely used as building blocks for functional peptides. We speculated that a new bis-cationic cyclic amino acid with cationic and peptide helix-promoting properties could become a useful building block for functional peptides. In this study, we designed a bis-cationic cyclic dAA containing a bispidine moiety, 9-amino-3,7-diazabicyclo[3.3.1]nonane-9-carboxylic acid (9-amino-bispidine-9-carboxylic acid; Abp), which is available for both solution phase and solid phase peptide synthesis (Fig. 1). That is to say, N-terminal Cbz- and Fmoc-

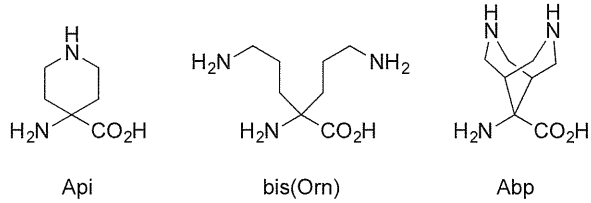

Fig. 1. Cationic amino acids.

* Corresponding authors. Tel.: +81 3 3700 1141; fax: +81 3 3707 6950; e-mail addresses: demizu@nihs.go.jp (Y. Demizu), masaaki@nihs.go.jp (M. Kurihara).

http://dx.doi.org/10.1016/j.tet.2015.02.076
0040-4020/

protected amino acids, Cbz-Abp-OH and Fmoc-Abp-OH, were synthesized. Furthermore, a tripeptide containing Abp (Boc-Leu-Abp-Ala-OMe) was prepared using the solution phase method, and its preferred conformation was analyzed by examining its Fourier transform infrared (FTIR) and nuclear magnetic resonance (NMR) spectra and performing molecular modeling.

2. Results and discussion

2.1. Synthesis of bis-cationic amino acids (Cbz-Abp-OH and Fmoc-Abp-OH) and heteropeptide

Our strategy for synthesizing N-terminal protected Cbz-Abp-OH (**6**) and Fmoc-Abp-OH (**7**) is shown in Scheme 1. In the first step, 1-Boc-4-piperidone was subjected to cyclization in the presence of benzylamine and paraformaldehyde to afford the 3,7-diazabicyclo [3.3.1]nonan-9-one derivative **1**.[10] The *N*-Benzyl group of **1** was replaced with a Boc group to give **2**, and then the hydantoin **3** was obtained from **2** via a Bücherer–Bergs procedure that resulted in a high yield. The conditions employed for the di-Boc protection of the hydantoin **3** are summarized in Table 1. As shown in entries 1–4, the use of several organic bases gave a mixture of the di- and mono-Boc protected hydantoins **4** and **5**, but the use of potassium carbonate, an inorganic base, gave only the mono-Boc product **5** (entry 5). Conversely, the di-Boc product **4** was exclusively obtained when trimethylpyridine (TMP) was used as a base (entry 6). The hydrolysis of **4** with aqueous LiOH gave an N- and C-terminal-free amino acid,[11] and subsequent Cbz protection afforded the side-chain Boc-protected amino acid Cbz-Abp-OH (**6**). The Fmoc-protected amino acid Fmoc-Abp-OH (**7**) was obtained by using Fmoc-OSu instead of Cbz-OSu.

Table 1
Di-Boc protection of the hydantoin **3**

Entry	Conditions	Yield of **4** (%)	Yield of **5** (%)
1	DIPEA, DMAP, THF	9	28
2	Et_3N, DMAP, THF	16	46
3	DBU, DMAP, THF	35	26
4	DABCO, DMAP, THF	37	24
5	K_2CO_3, acetone	0	75
6	TMP, THF	93	0

(HATU)/1-hydroxy-7-azabenzotriazole (HOAt) as a coupling reagent (Scheme 2).

2.2. Conformational analysis of the tripeptide 9

The FTIR spectra of peptides **8** and **9** in the NH-stretching region (amide A 3250–3500 cm^{-1}) were measured in $CDCl_3$ solution, as shown in Fig. 2. The band of the tripeptide **9** seen in the 3427 cm^{-1} region was assigned to free peptide NH groups, and the band observed in the 3350 cm^{-1} region was assigned to a peptide NH group with an N–H···O=C intramolecular hydrogen bond (Fig. 2a). This IR spectrum was very similar to those exhibited by 3_{10}-helical peptides containing β-turn structures in solution.[12] Whereas, in the spectrum of the dipeptide **8**, the single band at the 3427 cm^{-1} region was observed, indicating that the dipeptide **8** was not folded into the turn structure.

Fig. 3 shows a solvent perturbation experiment in which the tripeptide **9** was treated with the strong H-bond acceptor solvent dimethyl sulfoxide (DMSO) (0–10% (*v*/*v*)). Two NH (N_1–H and N_2–H) chemical shifts were found to be sensitive (solvent-exposed NH groups) to the addition of DMSO. The latter results demonstrate

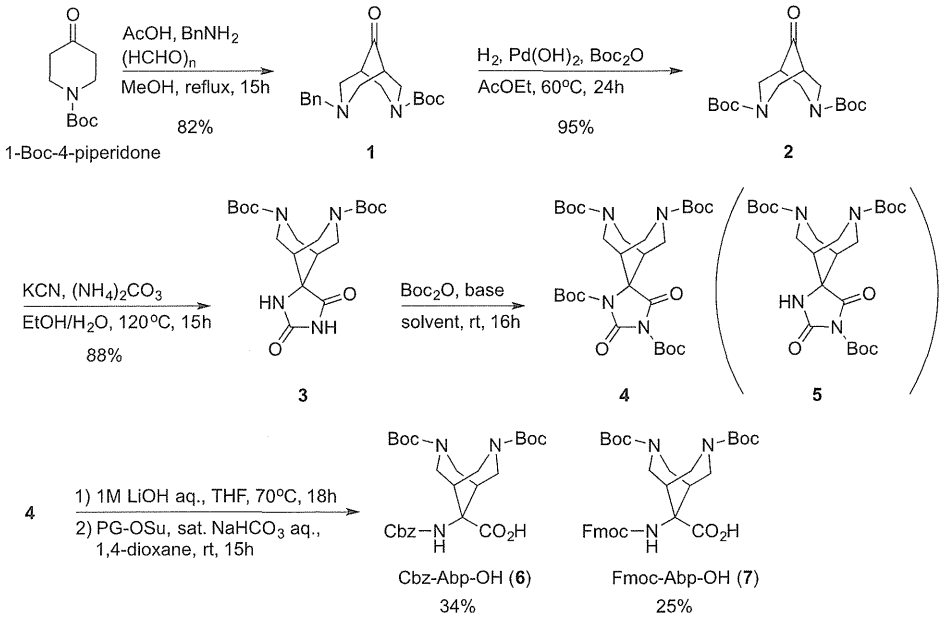

Scheme 1. Synthesis of bis-cationic cyclic α,α-disubstituted amino acids.

Then, the dipeptide Cbz-Abp-Ala-OMe (**8**) and the tripeptide Cbz-Leu-Abp-Ala-OMe (**9**), both of which contained Abp residues, were synthesized by conventional solution phase methods using 1-(3-dimethylaminopropyl)-3-ethylcarbodiimide (EDC), hydrochloride/1-hydroxybenzotriazole (HOBt) hydrate, or *O*-(7-azabenzotriazol-1-yl)-1,1,3,3-tetramethyluronium hexafluorophosphate that these two NH protons were exposed by the solvent used for the NMR, suggesting that are not intramolecularly hydrogen bonded. These findings are indicative of a β-turn or a 3_{10}-helical structure, in which the two NH groups (N_1–H and N_2–H) at the N-terminus of the peptide are freely solvated (not intramolecularly hydrogen bonded) peptide NH groups[13] (Fig. 4).

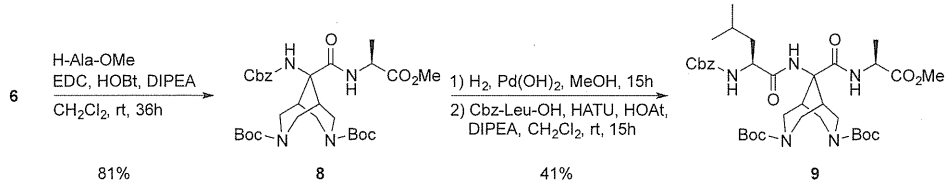

Scheme 2. Synthesis of the dipeptide **8** and the tripeptide **9**.

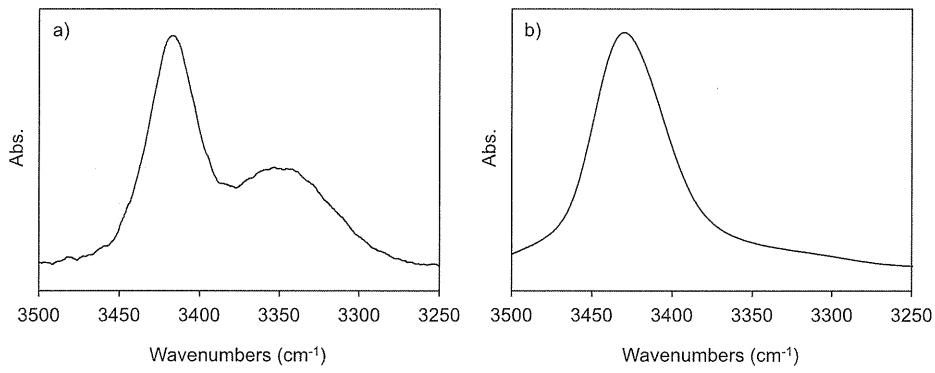

Fig. 2. IR spectra of (a) the tripeptide **9** and (b) the dipeptide **8** in $CDCl_3$ solution. Peptide concentration: 2.0 mM.

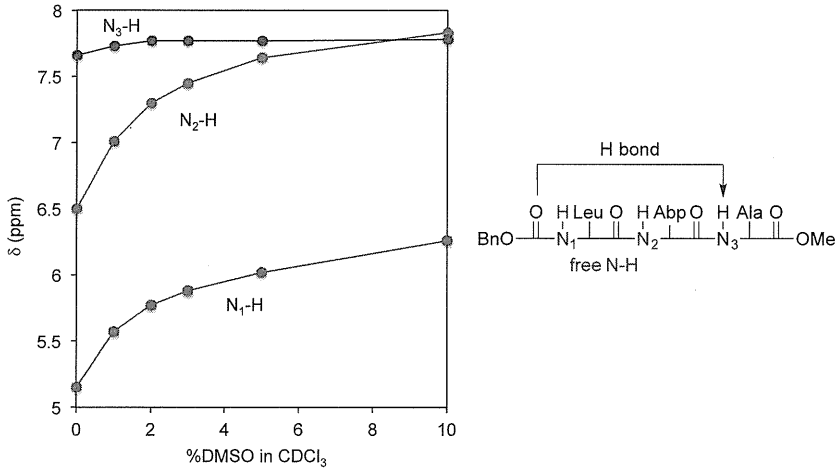

Fig. 3. ^{1}H NMR experiment involving the addition of DMSO to a $CDCl_3$ solution of tripeptide **9**. Plots of NH chemical shifts in the ^{1}H NMR spectra of **9** as a function of the percentage of DMSO (*v*/*v*) added to the $CDCl_3$ solution. Peptide concentration: 1.0 mM.

Conformational calculations for the tripeptide **9** were performed using the software package MacroModel ver. 10.0 (Schrodinger, Inc.). The Monte Carlo multiple minimum method and AMBER* force field were used to find the peptide's global minimum energy conformation. The peptide's extended conformation was used as the initial structure, and 20,000 conformers were optimized. The global minimum energy conformation of **9** was found to be a type III β-turn structure; i.e., a single 3_{10}-helix turn. The N-terminal carbonyl group (Boc group) served as thy hydrogen bond acceptor. Thus, the N-terminal protecting groups of helical peptides (including β-turn peptides) can generally work as the hydrogen bond acceptor in solution and in the crystalline state.[3d] This calculated structure was supported by our findings regarding the conformation of **9** in solution.

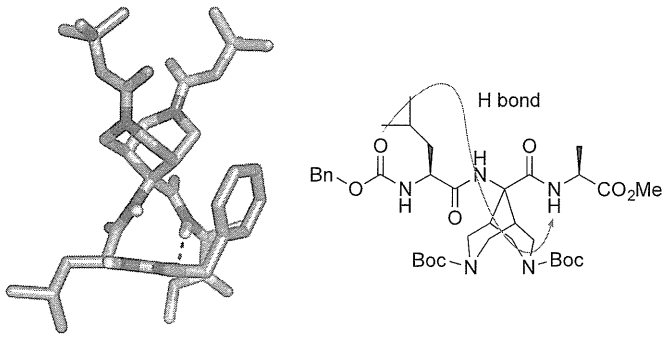

Fig. 4. The calculated conformation and hydrogen bonding pattern of the tripeptide **9**.

3. Conclusion

In summary, we have designed and synthesized a new biscationic cyclic amino acid, 9-amino-3,7-diazabicyclo[3.3.1]nonane-9-carboxylic acid (9-amino-bispidine-9-carboxylic acid; Abp), which is available for both solution phase and solid phase peptide synthesis and has peptide helix-promoting abilities. Furthermore, a tripeptide

containing an Abp residue, Cbz-Leu-Abp-Ala-OMe (**9**), was also prepared, and its dominant conformation was analyzed by examining its NMR and IR spectra and performing molecular modeling. The tripeptide **9** formed a β-turn structure as its preferred conformation in solution. Various acyclic and cyclic α,α-disubstituted amino acids having the helix promoting property generally act as β-turn inducers in the tripeptide sequence.[14] In this work, the tripeptide Cbz-Leu-Abp-Ala-OMe (**9**) containing Abp also formed a type III β-turn structure as its preferred conformation in solution and in the global minimum energy conformation. This alternating Leu-Abp-Ala segment forming the turn structure would give a helical structure in the longer sequences. The helix-promoting amino acid Abp is expected to be a valuable tool for producing biologically active molecules, such as drug delivery system carriers and antimicrobial peptides.

4. Experimental

4.1. General methods

^{1}H and ^{13}C NMR spectra were recorded on a *Varian AS 400* or a *JNM-ECA 600* spectrometer in $CDCl_3$, CD_3OD, or DMSO-d_6. FTIR spectra were recorded on a *JASCO FT/IR-4100* spectrometer at a resolution of 1 cm^{-1}. A mean of 64 scans were obtained for the solution ($CDCl_3$) method, and a NaCl cell path length of 0.1 mM was employed. Electrospray ionization mass spectrometry spectra were acquired on a *SHIMADZU* liquid chromatography mass spectrometry ion-trap time-of-flight spectrometer.

*4.1.1. Synthesis of compound **2**.* A suspension of **1** (3.3 g, 10.0 mmol), 20% $Pd(OH)_2$ (200 mg), and Boc_2O (2.6 g, 12.0 mmol) in AcOEt (50 mL) was vigorously stirred under an H_2 atmosphere at 60 °C for 24 h. After filtration of the Pd-catalyst, the filtrate was concentrated in vacuo, and the resultant residue was purified by column chromatography on silica gel (*n*-hexane:AcOEt=3:1) to give **2** (3.2 g, 95%) as a white solid. White solid; Mp 163–165 °C; IR ($CDCl_3$, cm^{-1}) 2976, 2938, 1736, 1690; ^{1}H NMR (600 MHz, CD_3OD) δ 3.94–4.03 (m, 4H), 3.32 (dd, *J*=9, 27 Hz, 2H), 3.23 (dd, *J*=12, 42 Hz, 2H), 1.90 (br s, 2H), 1.42 (s, 18H); ^{13}C NMR (100 MHz, CD_3OD) δ 155.7, 94.2, 91.1, 79.6, 36.4, 27.4; [HR-ESI(+)]: *m/z* calcd for $C_{17}H_{28}N_2O_5Na$ $[M+Na]^+$ 363.1890, found 363.1874.

*4.1.2. Synthesis of compound **3**.* A mixture of **2** (2.5 g, 7.3 mmol), $(NH_4)_2CO_3$ (2.3 g, 24.2 mmol), and KCN (774 mg, 11.9 mmol) in 50% aqueous EtOH (10 mL) was stirred at 120 °C in a sealed tube for 15 h. After removing the EtOH, the suspension was filtered off, and the precipitate was washed with a small portion of water to give the hydantoin **3** (2.5 g, 88%) as a white solid. White solid; Mp 234–236 °C; IR ($CDCl_3$, cm^{-1}) 3248, 2979, 1765, 1729, 1683; ^{1}H NMR (600 MHz, DMSO-d_6) δ 10.87 (s, 1H), 8.66 (s, 1H), 3.90 (δ, 1H), 3.83 (d, 1H), 3.82 (d, 1H), 3.66 (d, 1H), 3.54 (d, 1H), 3.34 (br s, 1H), 3.27 (d, 1H), 3.15 (d, 1H), 1.92 (d, 2H), 1.38 (s, 6H), 1.35 (s, 12H); ^{13}C NMR (100 MHz, DMSO-d_6) δ 176.6, 156.5, 154.7, 79.1, 61.4, 46.4, 45.7, 45.3, 44.8, 34.8, 28.7; [HR-ESI(+)]: *m/z* calcd for $C_{19}H_{30}N_4O_6Na$ $[M+Na]^+$ 433.2058, found 433.2023.

*4.1.3. Synthesis of compound **4**.* A solution of **3** (1.0 g, 2.4 mmol), TMP (1.6 mL, 12.2 mmol), and $(Boc)_2O$ (10.6 g, 48.7 mmol) in THF (20 mL) was stirred at room temperature for 16 h. After removing the THF and TMP, the resultant residue was purified by column chromatography on silica gel (*n*-hexane:AcOEt=3:1) to give the di-Boc protected hydantoin **4** (1.4 g, 93%) as colorless crystals. White solid; Mp 248–250 °C; IR ($CDCl_3$, cm^{-1}) 2980, 2920, 1770, 1660; ^{1}H NMR (600 MHz, $CDCl_3$) δ 4.03 (dd, *J*=18, 36 Hz, 2H), 3.92 (t, *J*=18 Hz, 2H), 3.66 (dd, *J*=12, 48 Hz, 2H), 3.48 (dd, *J*=18, 36 Hz, 2H), 2.18 (br s, 1H), 2.01 (br s, 1H), 1.53 (s, 9H), 1.51 (s, 9H), 1.43 (s, 9H), 1.41 (s, 9H); ^{13}C NMR (100 MHz, $CDCl_3$) δ 176.6, 155.1, 155.0, 154.9, 150.8, 146.2, 85.4, 85.0, 79.5, 67.3, 66.7, 46.7, 45.8, 45.1, 43.4, 35.5, 28.6, 28.3, 27.2, 24.2, 20.1; [HR-ESI(+)]: *m/z* calcd for $C_{24}H_{46}N_4O_8Na$ $[M+Na]^+$ 633.3106, found 633.3041.

*4.1.4. Spectroscopic data for the mono-Boc protected hydantoin **5**.* White solid; Mp 260–262 °C; IR ($CDCl_3$, cm^{-1}) 3310, 2976, 2930, 1770, 1690; ^{1}H NMR (600 MHz, $CDCl_3$) δ 7.79 (br s, 1H), 3.98–4.19 (m, 4H), 3.72 (dd, *J*=18, 48 Hz, 2H), 3.24 (dd, *J*=18, 54 Hz, 2H), 1.88 (br s, 2H), 1.51 (s, 9H), 1.48 (s, 18H); ^{13}C NMR (100 MHz, $CDCl_3$) δ 169.9, 154.9, 154.6, 152.1, 145.7, 86.3, 80.3, 80.0, 69.6, 60.5, 53.8, 45.7, 45.3, 44.6, 44.1, 35.2, 29.3, 28.4, 27.8, 21.1; [HR-ESI(+)]: *m/z* calcd for $C_{24}H_{38}N_4O_8Na$ $[M+Na]^+$ 533.2582, found 533.2537.

*4.1.5. Synthesis of compound **6**.* A solution of **4** (100 mg, 0.16 mmol) in 1 M aqueous LiOH (1.0 mL) and THF (1.0 mL) was stirred at 70 °C for 18 h. After the solution had been neutralized with 3% aqueous HCl, the THF was evaporated. Then, the aqueous solution was washed with Et_2O, before being concentrated in vacuo. Cbz-OSu (122.4 mg, 0.49 mmol), saturated aqueous $NaHCO_3$ (1.2 mL), and 1,4-dioxane (2.4 mL) were added to the resultant residue, and the solution was stirred at room temperature for 15 h. After removing the 1,4-dioxane, the solution was acidified with 3% aqueous HCl, extracted with AcOEt, and dried over Na_2SO_4. The solvent was then removed, and the residue was purified by column chromatography on silica gel (*n*-hexane: AcOEt=1: 3 in the presence of 1% AcOH) to give the Cbz-protected amino acid Cbz-Abp-OH **6** (29 mg, 34%) as a white solid. White solid; Mp 156–158 °C; IR ($CDCl_3$, cm^{-1}) 3309, 2986, 2880, 1740, 1680, 1529; ^{1}H NMR (600 MHz, $CDCl_3$) δ 7.21–7.29 (m, 5H), 6.06 (br s, 1H), 5.02 (s, 2H), 3.78–4.12 (m, 4H), 3.23–3.36 (m, 4H), 2.67 (br s, 1H), 2.47 (br s, 1H) 1.35 (s, 18H); ^{13}C NMR (100 MHz, DMSO-d_6) δ 173.3, 155.6, 154.9, 154.6, 137.5, 129.1, 128.6, 128.4, 79.1, 66.1, 58.6, 46.9, 45.9, 45.5, 44.5, 32.6, 32.3, 28.8; [HR-ESI(+)]: *m/z* calcd for $C_{26}H_{37}N_3O_8Na$ $[M+Na]^+$ 542.2473, found 542.2424.

*4.1.6. Spectroscopic data for the Fmoc-protected amino acid **7**.* White solid; Mp 257–259 °C; IR ($CDCl_3$, cm^{-1}) 3291, 2978, 2931, 1802, 1767, 1686; ^{1}H NMR (600 MHz, $CDCl_3$) δ 7.73 (d, *J*=7.2 Hz, 2H), 7.52 (d, *J*=7.2 Hz, 2H), 7.38 (t, *J*=7.6 Hz, 2H), 7.28 (t, *J*=7.6 Hz, 2H), 5.39 (br s, 1H), 4.46 (br s, 1H), 4.20 (d, *J*=7.2 Hz, 2H), 3.94–4.06 (m, 4H), 3.01–3.40 (m, 4H), 2.74 (br s, 1H), 2.51 (br s, 1H), 1.43 (s, 9H), 1.39 (s, 9H); ^{13}C NMR (100 MHz, $CDCl_3$) δ 175.6, 155.1, 154.8, 141.5, 127.9, 127.7, 124.8, 120.0, 80.1, 71.7, 66.9, 58.9, 47.2, 46.3, 45.2, 44.9, 28.6, 28.4, 22.7, 20.8; [HR-ESI(+)]: *m/z* calcd for $C_{33}H_{41}N_3O_8Na$ $[M+Na]^+$ 630.2786, found 630.2707.

*4.1.7. Synthesis of the dipeptide **8**.* A mixture of EDC (83 mg, 0.47 mmol), HOBt (66 mg, 0.47 mmol), DIPEA (183 μL, 1.08 mmol), L-alanine methyl ester hydrochloride (50 mg, 0.36 mmol), and **7** (62.2 mg, 0.12 mmol) in CH_2Cl_2 (2 mL) was stirred at room temperature for 36 h. The solution was then washed with 3% aqueous HCl, saturated aqueous $NaHCO_3$, and brine, before being dried over Na_2SO_4. After the solvent had been removed, the residue was purified by column chromatography on silica gel (*n*-hexane:AcOEt=2:1) to give the dipeptide **8** (58 mg, 81%). White solid; Mp 166–168 °C; IR ($CDCl_3$, cm^{-1}) 3427, 2979, 2929, 2872, 1741, 1688; ^{1}H NMR (400 MHz, $CDCl_3$) δ 7.28–7.37 (m, 6H), 5.38 (br s, 0.5H), 5.33 (br s, 0.5H), 5.09 (dd, *J*=12, 18.8 Hz, 2H), 4.48–4.51 (m, 1H), 3.97–4.17 (m, 4H), 3.71 (s, 3H), 3.24–3.42 (m, 4H), 2.63 (br s, 2H), 1.42 (s, 9H), 1.41 (s, 9H), 1.28 (s, *J*=4.4 Hz, 3H); ^{13}C NMR (100 MHz, $CDCl_3$) δ 173.0, 170.3, 156.0, 155.2, 154.7, 135.9, 128.6, 128.4, 128.1, 79.8, 67.2, 60.4, 58.6, 52.4, 48.2, 46.4, 45.2, 44.8, 43.9, 32.6, 32.4, 31.6, 28.5, 28.4, 28.3, 21.1; [HR-ESI(+)]: *m/z* calcd for $C_{30}H_{44}N_4O_9Na$ $[M+Na]^+$ 627.3001, found 627.2963.

*4.1.8. Synthesis of the tripeptide **9**.* A mixture of **8** (104 mg, 0.17 mmol) and 20% $Pd(OH)_2$ (10 mg) in MeOH (10 mL) was

rigorously stirred under an H_2 atmosphere at room temperature for 15 h and then filtrated. The filtrate was concentrated in vacuo to give a crude amine, which was used for the next reaction without further purification. A mixture of HATU (233 mg, 0.61 mmol), HOAt (83 mg, 0.61 mmol), DIPEA (260 μL, 1.53 mmol), the above-mentioned amine, and Cbz-protected L-leucine (137 mg, 0.52 mmol) in CH_2Cl_2 (10 mL) was stirred at room temperature for 15 h. The solution was washed with 3% aqueous HCl, saturated aqueous $NaHCO_3$, and brine, before being dried over Na_2SO_4. After the solvent had been removed, the residue was purified by column chromatography on silica gel (*n*-hexane:AcOEt=1:1) to give the tripeptide **9** (52 mg, 41%). White solid; Mp 180–182 °C; IR ($CDCl_3$, cm^{-1}) 3427, 3350, 2958, 2932, 1734, 1691; ^1H NMR (400 MHz, $CDCl_3$) δ 7.72 (br s, 1H), 7.27–7.33 (m, 5H), 6.83 (br s, 1H), 5.30 (br s, 1H), 5.09 (dd, J=8.4, 23.2 Hz, 2H), 4.41–4.46 (m, 1H), 3.93–4.16 (m, 5H), 3.64 (s, 3H), 3.13–3.48 (m, 4H), 2.94 (br s, 1H), 2.59 (br s, 1H), 1.66–1.71 (m, 3H), 1.40–1.47 (m, 21H), 0.92 (br s, 6H); ^{13}C NMR (100 MHz, $CDCl_3$) δ 173.9; 173.0, 170.2, 156.6, 156.2, 154.7; 136.3, 128.7, 128.3, 128.2, 79.9, 67.6, 67.1, 59.8, 54.2, 52.4, 48.2, 46.4, 45.2, 44.9, 41.5, 40.2, 28.6, 28.4, 24.8, 22.9, 22.8, 21.9; [HR-ESI(+)]: *m/z* calcd for $C_{36}H_{55}N_5O_{10}Na$ $[M+Na]^+$ 740.3841, found 740.3804.

Acknowledgements

This study was supported, in part, by JSPS KAKENHI Grant Number 26460169 (Y.D.), by a Grant-in-Aid from the Tokyo Biochemical Research Foundation (Y.D.), and scholarship support from the Shoshisha Foundation (H.Y.).

References and notes

1. (a) Potocky, T. B.; Menon, A. K.; Gellman, S. H. *J. Am. Chem. Soc.* **2005**, *127*, 3686–3687; (b) Oehlke, J.; Birth, P.; Klauschenz, E.; Wiesner, B.; Beyermann, M.; Oksche, A.; Bienert, M. *Eur. J. Biochem.* **2002**, *269*, 4025–4032; (c) Wada, S.; Tsuda, H.; Okada, T.; Urata, H. *Bioorg. Med. Chem. Lett.* **2011**, *21*, 5688–5691.
2. (a) Wada, S.; Urase, T.; Hasegawa, Y.; Ban, K.; Sudani, A.; Kawai, Y.; Hayashi, J.; Urata, H. *Bioorg. Med. Chem.* **2014**, *22*, 6776–6780; (b) Azzarito, V.; Long, K.; Murphy, N. S.; Wilson, A. J. *Nat. Chem.* **2013**, *5*, 161–173; (c) Yamashita, H.; Demizu, Y.; Shoda, T.; Sato, Y.; Oba, M.; Tanaka, M.; Kurihara, M. *Bioorg. Med. Chem.* **2014**, *22*, 2403–2408; (d) Nagakubo, T.; Demizu, Y.; Kanda, Y.; Misawa, T.; Shoda, T.; Okuhira, K.; Sekino, Y.; Naito, M.; Kurihara, M. *Bioconjugate Chem.* **2014**, *25*, 1921–1924.
3. (a) Brown, R. A.; Diemer, V.; Webb, S. J.; Clayden, J. *Nat. Chem.* **2013**, *5*, 853–860; (b) Tanaka, M. *Chem. Pharm. Bull.* **2007**, *55*, 349–358; (c) Royo, S.; Borggraeve, W. M. D.; Peggion, C.; Formaggio, F.; Crisma, M.; Jiménez, A. I.; Cativiela, C.; Toniolo, C. *J. Am. Chem. Soc.* **2005**, *127*, 2036–2037; (d) Demizu, Y.; Yamashita, H.; Yamazaki, N.; Sato, Y.; Doi, M.; Tanaka, M.; Kurihara, M. *J. Org. Chem.* **2013**, *78*, 12106–12113.
4. (a) Wang, S.; Otani, Y.; Liu, X.; Kawahata, M.; Yamaguchi, K.; Ohwada, T. *J. Org. Chem.* **2014**, *79*, 5287–5300; (b) Imamura, Y.; Umezawa, N.; Osawa, S.; Shimada, N.; Higo, T.; Yokoshima, S.; Fukuyama, T.; Iwatsubo, T.; Kato, N.; Tomita, T.; Higuchi, T. *J. Med. Chem.* **2013**, *56*, 1443–1454; (c) Horne, W. S.; Gellman, S. H. *Acc. Chem. Res.* **2008**, *41*, 1399–1408; (d) Seebach, D.; Gardiner, J. *Acc. Chem. Res.* **2008**, *41*, 1366–1375.
5. (a) Tanaka, M.; Nishimura, S.; Oba, M.; Demizu, Y.; Kurihara, M.; Suemune, H. *Chem.—Eur. J.* **2003**, *9*, 3082–3090; (b) Imawaka, N.; Tanaka, M.; Suemune, H. *Helv. Chim. Acta* **2000**, *83*, 2823–2835; (c) Benedetti, E. *Biopolymers (Pept. Sci.)* **1996**, *40*, 3–44.
6. (a) Yeo, D. J.; Warriner, S. L.; Wilson, A. J. *Chem. Commun.* **2013**, 9131–9133; (b) Yamaguchi, H.; Kodama, H.; Osada, S.; Kato, F.; Jelokhani-Niaraki, M.; Kondo, M. *Biosci. Biotechnol. Biochem.* **2003**, *67*, 2269–2272.
7. (a) Cho, J.; Tanaka, M.; Sato, S.; Kinbara, K.; Aida, T. *J. Am. Chem. Soc.* **2010**, *132*, 13176–13178; (b) Ousaka, N.; Inai, Y.; Kuroda, R. *J. Am. Chem. Soc.* **2008**, *130*, 12266–12267; (c) Oba, M.; Tanaka, M.; Takano, Y.; Suemune, H. *Tetrahedron* **2005**, *61*, 593–598; (d) Yokum, T. S.; Elzer, P. H.; McLaughlin, M. L. *J. Med. Chem.* **1996**, *39*, 3603–3605.
8. Aussedat, B.; Chassaing, G.; Lavielle, S.; Burlina, F. *Tetrahedron Lett.* **2006**, *47*, 3723–3726.
9. Aussedat, B.; Dupont, E.; Sagan, S.; Joliot, A.; Lavielle, S.; Chassaing, G.; Burlina, F. *Chem. Commun.* **2008**, 1398–1400.
10. Huttenloch, O.; Laxman, E.; Waldmann, H. *Chem. Commun.* **2002**, 673–675.
11. Wysong, C. L.; Yokum, T. S.; Morales, G. A.; Gundry, R. L.; McLaughlin, M. L.; Hammer, R. P. *J. Org. Chem.* **1996**, *61*, 7650–7651.
12. (a) Crisma, M.; Bonora, G. M.; Toniolo, C.; Benedetti, E.; Bavoso, A.; Di Blasio, B.; Pavone, V.; Pedone, C. *Int. J. Biol. Macromol.* **1988**, *10*, 300–304; (b) Benedetti, E.; Barone, V.; Bavoso, A.; Di Blasio, B.; Lelj, F.; Pavone, V.; Pedone, C.; Bonora, G. M.; Toniolo, C.; Leplawy, M. T.; Kaczmarek, K.; Redlinski, A. *Biopolymers* **1988**, *27*, 357–371.
13. (a) Polese, A.; Formaggio, F.; Crisma, M.; Valle, G.; Toniolo, C.; Bonora, G. M.; Broxterman, Q. B.; Kamphuis, J. *Chem.—Eur. J.* **1996**, *2*, 1104–1111; (b) Demizu, Y.; Doi, M.; Kurihara, M.; Maruyama, T.; Suemune, H.; Tanaka, M. *Chem.—Eur. J.* **2012**, *18*, 2430–2439; (c) Demizu, Y.; Yabuki, Y.; Doi, M.; Sato, Y.; Tanaka, M.; Kurihara, M. *J. Pept. Sci.* **2012**, *18*, 466–475.
14. (a) Gatos, M.; Formaggio, F.; Crisma, M.; Toniolo, C.; Bonora, G. M.; Benedetti, Z.; Blasio, B. D.; Iacovino, R.; Santini, A.; Saviano, M.; Kamphuis, J. *J. Pept. Sci.* **1997**, *3*, 110–122; (b) Jiménez, A. I.; Cativiela, C.; Aubry, A.; Marraud, M. *J. Am. Chem. Soc.* **1998**, *120*, 9452–9459; (c) Formaggio, F.; Crisma, M.; Toniolo, C.; Tchertanov, L.; Guilhem, J.; Mazaleyrat, J.-P.; Gaucher, A.; Wakselman, M. *Tetrahedron* **2000**, *56*, 8721–8734; (d) Haldar, D.; Drew, M. G. B.; Banerjee, A. *Tetrahedron* **2007**, *63*, 5561–5566.

SCIENTIFIC REPORTS

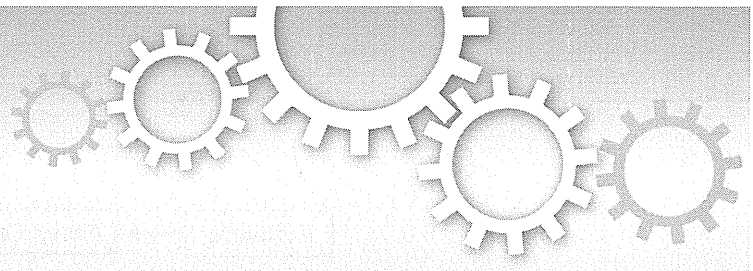

OPEN

SUBJECT AREAS:
METABOLOMICS
ENVIRONMENTAL SCIENCES

Received
17 February 2014

Accepted
15 July 2014

Published
5 August 2014

Correspondence and requests for materials should be addressed to Y.Ka (kanda@nihs.go.jp)

NAD-dependent isocitrate dehydrogenase as a novel target of tributyltin in human embryonic carcinoma cells

Shigeru Yamada[1], Yaichiro Kotake[2], Yosuke Demizu[3], Masaaki Kurihara[3], Yuko Sekino[1] & Yasunari Kanda[1]

[1]Division of Pharmacology, National Institute of Health Sciences, Tokyo, Japan, [2]Graduate School of Biomedical and Health Sciences, Hiroshima University, Hiroshima, Japan, [3]Division of Organic Chemistry, National Institute of Health Sciences, Tokyo, Japan.

Tributyltin (TBT) is known to cause developmental defects as endocrine disruptive chemicals (EDCs). At nanomoler concentrations, TBT actions were mediated by genomic pathways via PPAR/RXR. However, non-genomic target of TBT has not been elucidated. To investigate non-genomic TBT targets, we performed comprehensive metabolomic analyses using human embryonic carcinoma NT2/D1 cells. We found that 100 nM TBT reduced the amounts of α-ketoglutarate, succinate and malate. We further found that TBT decreased the activity of NAD-dependent isocitrate dehydrogenase (NAD-IDH), which catalyzes the conversion of isocitrate to α-ketoglutarate in the TCA cycle. In addition, TBT inhibited cell growth and enhanced neuronal differentiation through NAD-IDH inhibition. Furthermore, studies using bacterially expressed human NAD-IDH and *in silico* simulations suggest that TBT inhibits NAD-IDH due to a possible interaction. These results suggest that NAD-IDH is a novel non-genomic target of TBT at nanomolar levels. Thus, a metabolomic approach may provide new insights into the mechanism of EDC action.

Endocrine disruptive compounds (EDCs) have been studied extensively in environmental biology[1]. A large number of EDCs are known to cause genomic action via nuclear receptor. For example, xenoestrogens such as bisphenol A, genistein and diethylstilbestrol can bind to the estrogen receptor (ER) in the cell nucleus, followed by the alteration of gene expression[2,3]. In addition, EDCs induce the activation of non-genomic signaling pathways. For example, xenoestrogens increase intracellular calcium levels, activating eNOS and signaling cascades such as PI3K/AKT and MAPK[4–7]. Thus, both genomic and non-genomic pathways are required to understand the mechanism of EDC action.

Organotin compounds, such as tributyltin (TBT) are typical environmental contaminants and well known to cause developmental defects as EDCs. For example, TBT can cause increased fetal mortality, decreased fetal birth weights, and behavioral abnormalities in rat offspring[8,9]. Although the use of TBT has already been restricted, butyltin compounds, including TBT, can still be found in human blood at concentrations between 50 and 400 nM[10]. Several studies revealed that TBT activates retinoid X receptor (RXR) and/or peroxisome proliferator-activated receptor γ (PPARγ). These genomic transcriptional activations result in developmental effects, such as the imposex in many marine species[11–13] and the enhancement of adipocyte differentiation in mammals[14,15]. These TBT actions involve a higher binding affinity compared to intrinsic ligands at nM concentrations. In addition to the genomic effects, non-genomic action of TBT has been also reported. For example, TBT has been reported to inhibit the steroid biosynthesis pathway, which is responsible for the production of estrogen and androgen[16–18]. Another report has shown that TBT inhibits mitochondrial F1F0 ATP synthase[19]. These data were obtained at μM concentrations. Thus, the mechanism of nM concentrations of TBT has not been elucidated at a non-genomic level. In a previous study, we reported that treatment with 100 nM TBT resulted in growth arrest by targeting the glycolytic systems of the human embryonic carcinoma cell line NT2/D1[20]. Therefore, we raised the possibility that nM concentrations of TBT may target other non-genomic pathways which are involved in energy metabolism.

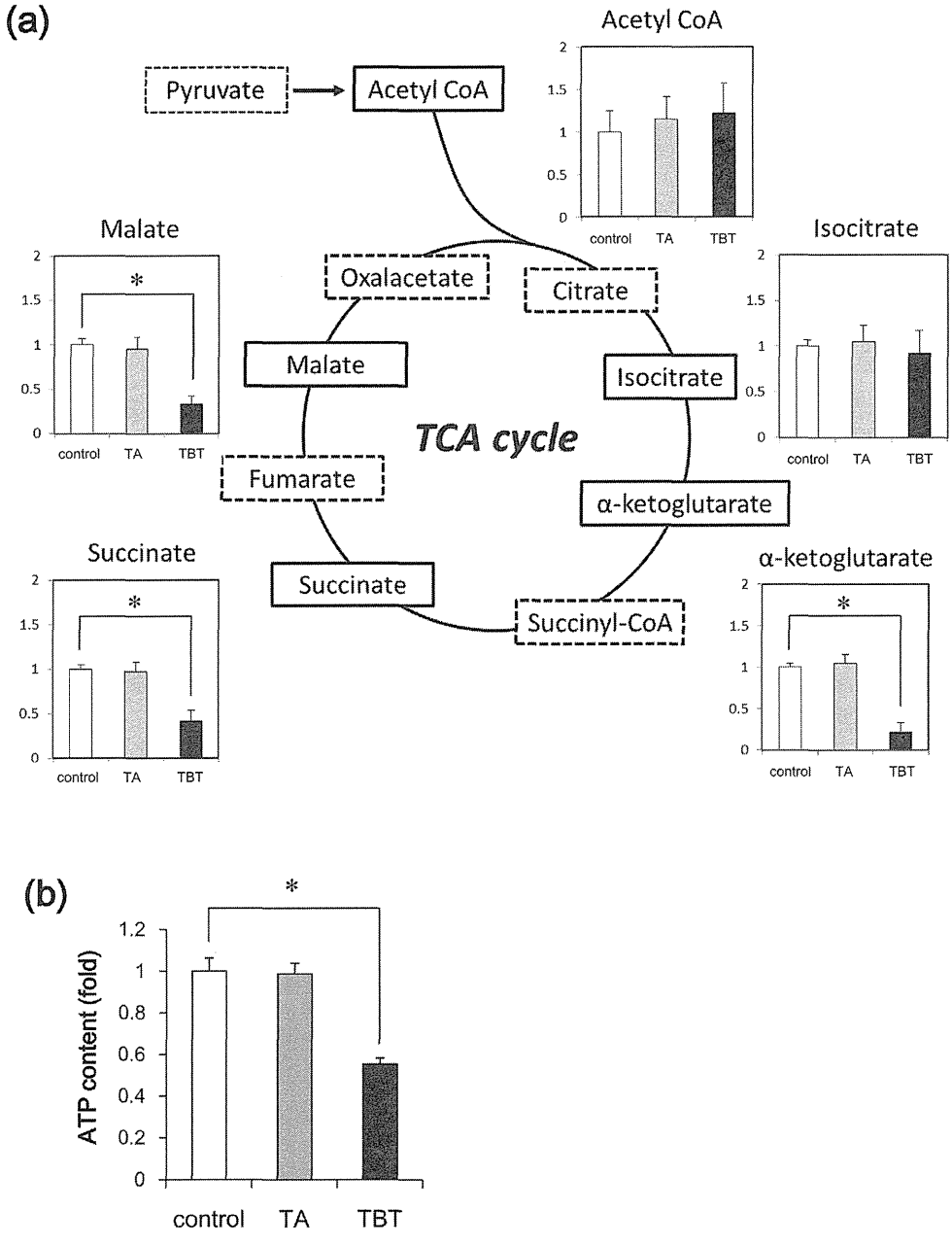

Figure 1 | Metabolomic analysis of NT2/D1 cells exposed to TBT. The cells were exposed to 100 nM TBT or TA for 24 h. (a) The levels of several metabolites, such as acetyl CoA, isocitrate, α-ketoglutarate, succinate and malate, were determined using CE-TOFMS. (b) The intracellular ATP content was determined in the lysed cells. * $P < 0.05$ compared with the corresponding control group.

In the present study, we investigated the molecular target of TBT at nM levels by comprehensive determination of the intracellular metabolites in NT2/D1 cells after TBT exposure. We found that exposure to 100 nM TBT reduced ATP production via NAD-dependent isocitrate dehydrogenase (NAD-IDH) in the cells. This NAD-IDH inhibition resulted in the reduction of the TCA cycle metabolites. In addition, TBT caused neural differentiation through an NAD-IDH-dependent mechanism. We report here that our metabolomic analysis revealed that NAD-IDH is a novel target of TBT in embryonic carcinoma cells.

Results

Metabolomic analysis of NT2/D1 cells exposed to TBT at nM levels. To investigate the non-genomic effects of a well-known endocrine disruptor TBT in human NT2/D1 embryonic carcinoma cells, we comprehensively determined intracellular metabolites using LC/MS. We found that exposure to 100 nM TBT reduced the amounts of TCA cycle components, such as α-ketoglutarate, succinate and malate (Figure 1a). The amounts of acetyl CoA and isocitrate were not changed. We also found that treatment with 100 nM TBT reduced the ATP content of the cells (Figure 1b). In contrast to TBT, exposure to the less toxic tin acetate (TA) did not affect the amount of each metabolite. These data suggest that TBT exposure decreases the amounts of TCA cycle metabolites, resulting in a reduction of ATP content.

NAD-IDH enzyme activity of NT2/D1 cells exposed to TBT at nM levels. Based on the results of the metabolomic analysis, we focused

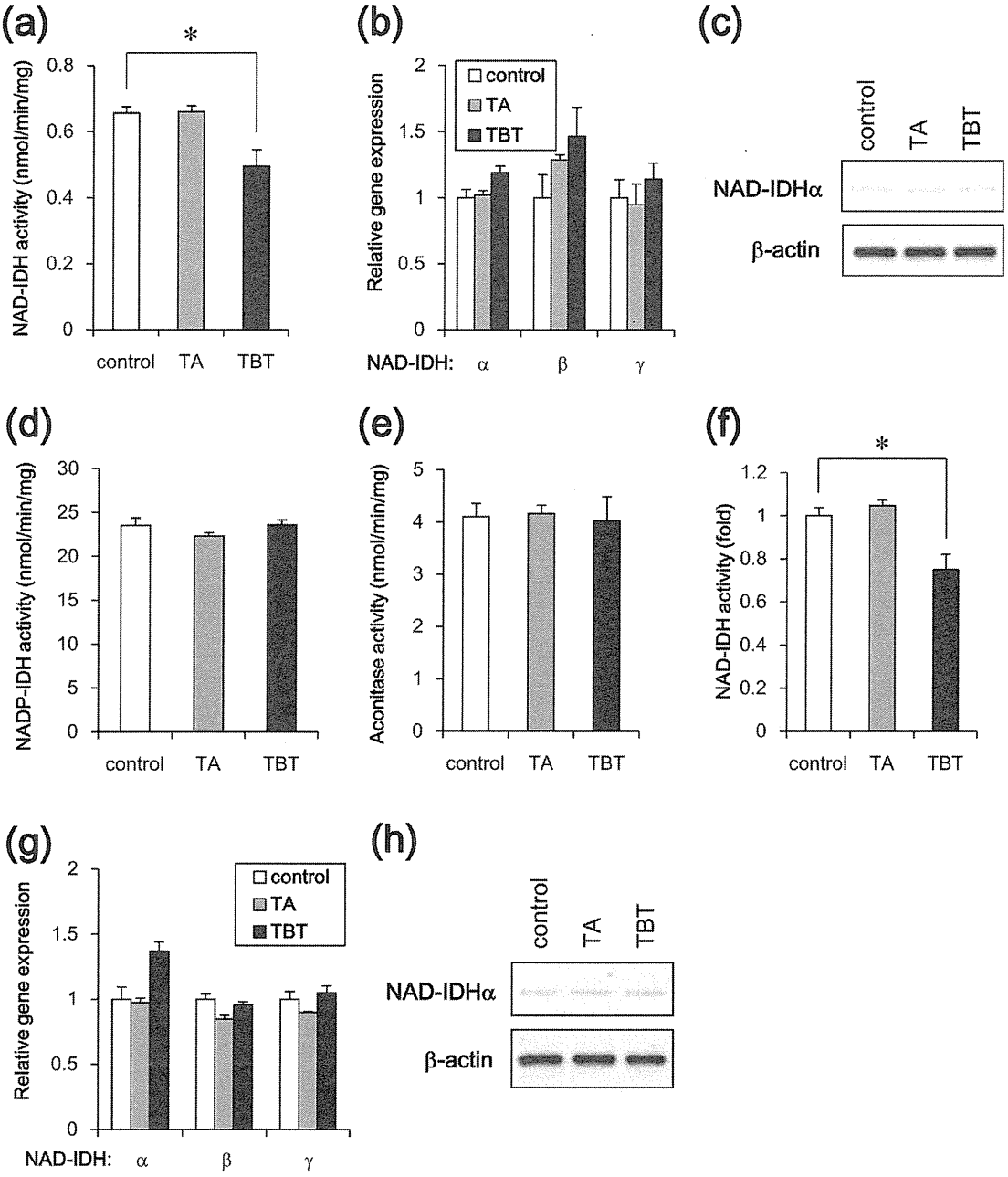

Figure 2 | Effect of TBT exposure on NAD-IDH enzyme activity in NT2/D1 cells. The cells were exposed to 100 nM TBT or TA for 24 h. (a) NAD-IDH activity was determined in the lysed cells. (b) The relative expressions of NAD-IDHα, β, and γ were measured using real-time PCR. The relative changes were normalized to the levels of RPL13. (c) The expression of NAD-IDHα protein was examined by western blot analysis using the anti-NAD-IDHα and anti-β-actin antibodies. Cropped blots were shown and the full-length blots were indicated in Supplementary Fig. 4. (d) NADP-IDH activity was determined in the lysed cells. (e) Aconitase activity was determined in the lysed cells. (f) To induce neuronal differentiation, the NT2/D1 cells were treated with 10 μM retinoic acid (RA) for 14 days. After exposure to 100 nM TBT for 24 h, NAD-IDH activity was determined in the lysed cells. (g) The relative expression levels of NAD-IDHα, β, and γ in the differentiated cells were measured using real-time PCR. The relative changes were normalized to the levels of RPL13. (h) The expression of NAD-IDHα protein was examined by western blot analysis using the anti-NAD-IDHα and anti-β-actin antibodies. Cropped blots were shown and the full-length blots were indicated in Supplementary Fig. 4. * $P < 0.05$ compared with the corresponding control group.

on isocitrate dehydrogenase, which catalyzes the conversion of isocitrate to α-ketoglutarate in the TCA cycle. Eukaryotes have different types of isocitrate dehydrogenases, such as NAD-dependent form (NAD-IDH; EC 1.1.1.41) and NADP-dependent form (NADP-IDH; EC 1.1.1.42)[21]. NAD-IDH is first rate-limiting enzyme in the TCA cycle and catalyzes an irreversible reaction, while NADP-IDH is involved in reversible reaction for biosynthesis via production of NADPH. As shown in Figure 2a, NAD-IDH activity was significantly reduced following TBT treatment. Since NAD-IDH is a heterotetramer composed of two α subunits (catalytic subunit), one β subunit and one γ subunit (regulatory subunit), we examined the expression of each subunit gene. Real-time PCR analysis showed

that the expression of the NAD-IDHα, β and γ genes was not significantly changed by TBT exposure (Figure 2b). The protein expression of catalytic α subunits was not also changed by TBT exposure (Figure 2c). TA exposure did not affect either the enzyme activity or the NAD-IDH expression. We next examined the effect of TBT on NADP-IDH. The activity of NADP-IDH was not affected by TBT exposure (Figure 2d). We further examined the activity of aconitase (EC 4.2.1.3.), which catalyzes the conversion of citrate to isocitrate in the TCA cycle. Aconitase activity was also not affected by TBT exposure (Figure 2e). Thus, these data suggest that the inhibitory effect of TBT is specific to NAD-IDH in the TCA cycle.

To investigate whether TBT cytotoxicity was caused by a genomic transcriptional regulation, we tested the effects of the protein synthesis inhibitor cycloheximide in NT2/D1 cells. Treatment with cycloheximide did not alter the inhibitory effects of TBT on NAD-IDH activity (Figure S1a) and intracellular ATP production (Figure S2a). Moreover, the PPARγ agonist rosiglitazone did not reduce NAD-IDH activity (Figure S1b) and ATP content (Figure S2b). These results suggest that transcriptional regulation is not involved in the inhibition of NAD-IDH activity by TBT.

To examine whether the effect of TBT was selective for embryonic cells, we used NT2/D1 cells that had differentiated in response to retinoic acid. We observed that TBT also inhibited NAD-IDH activity in the differentiated NT2/D1 cells (Figure 2f). Real-time PCR analysis showed that the expression of the NAD-IDHα, β, and γ genes was not significantly affected by TBT exposure (Figure 2g). The protein expression of catalytic α subunits was not also changed by TBT exposure (Figure 2h). TA exposure did not affect either the activity or the NAD-IDH expression. These data suggest that TBT reduces NAD-IDH enzyme activity regardless of the developmental stage of the embryonic carcinoma cells.

Neuronal differentiation of RA-treated NT2/D1 cells exposed to TBT at nM levels. It has been reported that ATP content decreases during the differentiation of human embryonic stem cells into neural stem cells (NSCs)[22]. Therefore, the reduction of ATP caused by TBT treatment might be involved in neuronal differentiation. Moreover, TBT has been reported to cause cell growth arrest in NT2/D1 cells[20]. Because cell growth is generally reduced during differentiation, we examined whether TBT affects the neuronal differentiation process in NT2/D1 cells. Real-time PCR analysis revealed that retinoic acid (RA)-treated NT2/D1 cells showed increased expression of the differentiation markers NeuroD and Math1, confirming that neural differentiation had occurred (Figure 3a). Furthermore, we observed that TBT exposure enhanced the expression levels of these neuronal differentiation markers. Treatment with rosiglitazone had little effect on their expression (Figure S3), suggesting that PPARγ is not involved in neuronal differentiation. Taken together, these data suggest that TBT promotes neuronal differentiation.

Effect of NAD-IDH knockdown on neuronal differentiation in RA-treated NT2/D1 cells. To further investigate whether the neuronal differentiation triggered by TBT exposure is through an NAD-IDH-dependent mechanism, we performed knockdown (KD) of NAD-IDHα, the catalytic subunit of NAD-IDH, using lentivirus-delivered shRNAs. Real-time PCR analysis showed that KD efficiency was approximately 40% (Figure 3b). Due to the partial KD of the NAD-IDHα gene, NAD-IDH activity decreased to a level (22%) comparable to its level following TBT inhibition (24%) (Figure 3c). Further reduction of NAD-IDH activity was not significantly observed after TBT exposure in the NAD-IDHα KD cells. Similar to the effect of TBT, NAD-IDHα KD also reduced the ATP content of the cells (Figure 3d), and caused cell growth inhibition (Figure 3e). Further inhibition of ATP content and cell growth was not significantly observed after TBT exposure in the NAD-IDHα KD cells, suggesting that the NAD-IDH is a possible target of TBT. In addition, we found that NAD-IDHα KD significantly upregulated the expression of the neuronal differentiation markers NeuroD and Math1 (Figure 3f). These data suggest that NAD-IDH mediates TBT-induced neuronal differentiation in embryonic NT2/D1 cells.

NAD-IDH enzyme activity in the brain of rats orally exposed to TBT at low doses. To examine whether the in vitro inhibitory effect of TBT on NAD-IDH is also observed in vivo, adult rats were orally exposed to TBT at doses of 5 and 50 mg/kg. NAD-IDH activity in the cerebral cortex was significantly reduced following exposure to both doses of TBT (Figure 4a). Real-time PCR analysis showed that the expression of the NAD-IDHα, β, and γ genes was not significantly affected by TBT (Figure 4b). The protein expression of catalytic α subunits was not also affected by TBT (Figure 4c). NADP-IDH and aconitase activities were not affected by exposure to either dose of TBT (Figure 4d and e). These data suggest that TBT inhibits NAD-IDH activity both in vitro and in vivo.

Reduction of recombinant hNAD-IDH enzyme activity in E. coli lysate treated with TBT at nM levels. To investigate the mechanism by which TBT inhibits NAD-IDH activity, we examined whether TBT possibly interacts with NAD-IDH or not. Since NAD-IDHα subunit alone has been reported to show no detectable IDH activity, we used an Escherichia coli co-expression system of recombinant human (h) NAD-IDHα,β,γ subunits[23]. As shown in Figure 5a, we confirmed the expression of α subunit of hNAD-IDH protein in the extracts of E. coli transformants using western blot analysis. To check the activity of the recombinant hNAD-IDH, we used irreversible and allosteric NAD-IDH regulators. ADP has been reported to activate NAD-IDH allosterically by lowering the Km for the substrate isocitrate[24]. As expected, ADP increased the activity of hNAD-IDH in our assay system. Conversely, Zn^{2+} has been reported to inhibit several metabolic enzymes, including NAD-IDH, in hepatocytes[25]. We confirmed that Zn^{2+} reduces hNAD-IDH activity. Then, we examined whether TBT directly inhibits hNAD-IDH activity by adding TBT to the E. coli extracts containing hNAD-IDH. Treatment with 100 nM TBT for 1 h significantly reduced the hNAD-IDH activity (Figure 5b). Treatment with TA had little effect. Taken together, these data suggest that TBT inhibits hNAD-IDH activity through its possible interaction, but again we can not be sure that it is through direct binding with the data we have.

***In silico* docking simulation analysis.** To further consider this possible interaction between TBT and hNAD-IDH, we estimate TBT accessibility into hNAD-IDH (EC 1.1.1.41) α and hNADP-IDH (EC 1.1.1.42) homodimers by homology modeling and docking studies. We show the overlaid structure of the calculated hNAD-IDHα and hNADP-IDH (Figure 6a). The ligand binding pocket of hNAD-IDHα was larger than that of hNADP-IDH (Figure 6b). In our docking simulation, TBT was able to access the hNAD-IDHα ligand-binding pocket, whereas the hNADP-IDH pocket was not spacious enough to accommodate TBT (Figure 6c and d). Thus, these studies suggest that the selective inhibition of NAD-IDH by TBT may be due to differences in the pocket volumes between hNAD-IDHα and hNADP-IDH.

Discussion

In the present study, we demonstrate that NAD-IDH is a novel non-genomic target of TBT at nM levels both in vitro and in vivo. We showed that exposure to nM concentrations of TBT reduced the activity of NAD-IDH due to its possible interaction. We also found that TBT exposure caused both inhibition of cell growth and enhancement of neuronal differentiation through its inhibitory effect of NAD-IDH.

Our data suggest that NAD-IDH is a novel target molecule of TBT action. NAD-IDH is a NAD-dependent form of IDH found in NT2/D1 cells and the rat brain (Figure 2–4). Because NAD-IDH is ubi-

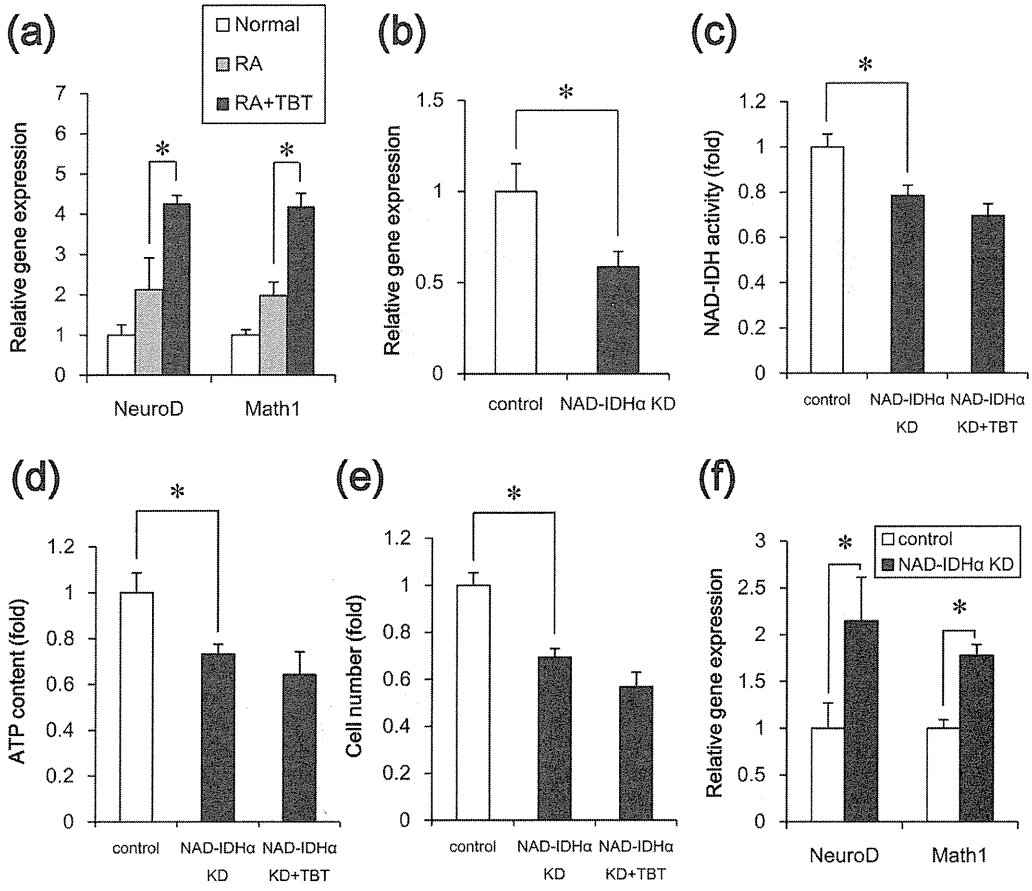

Figure 3 | Effect of TBT exposure or NAD-IDH knockdown on neuronal differentiation in RA-treated NT2/D1 cells. (a) After treatment with RA for 7 days, the cells were treated with RA in the presence of 100 nM TBT for an additional 7 days. The relative expression levels of the neuronal markers NeuroD and Math1 were measured using real-time PCR. The relative changes were determined following normalization to the levels of RPL13. (b–e) The cells were infected with lentiviruses containing a vector encoding a shRNA directed against NAD-IDHα or a scrambled sequence shRNA (control). The infected cells were subjected to selection with 0.5 μg/ml puromycin for 72 h and were then exposed to TBT at 100 nM for 24 h. (b) The relative expression of NAD-IDHα was measured using real-time PCR. The relative change in expression was normalized to the levels of RPL13. (c) NAD-IDH activity was determined in the lysed cells. (d) The intracellular ATP content was determined in the lysed cells. (e) Infected cells were seeded into 100 mm dishes and cultured for 24 h. Cell count was determined using a hemocytometer. (f) After treatment with RA for 7 days, followed by treatment with RA and the shRNA-containing lentiviruses for an additional 7 days, the relative expression levels of the neuronal markers NeuroD and Math1 were measured using real-time PCR. The relative changes were determined following normalization to the levels of RPL13. * $P < 0.05$ compared with the corresponding group.

quitously expressed, the toxicity of TBT might be observed in various cell types. Several TCA cycle enzymes have been reported to contribute to cell proliferation. For example, NADP-IDH plays a role for cell growth under hypoxic conditions in human glioblastoma cells[26]. Another study has shown that aconitase mediated cell proliferation via ATP production in human prostate carcinoma cells[27]. NAD-IDH has been shown to regulate the metabolic fluxes and the generation of ATP in the TCA cycle[28]. Therefore, it is likely that NAD-IDH is a target of TBT cytotoxicity and regulates cell growth in embryonic carcinoma cells.

In addition to cell growth inhibition, we also showed that neural differentiation is enhanced by TBT exposure or NAD-IDH inhibition (Figure 3). Consistent with our data, overexpression of NAD-IDHα has been shown to reduce neuronal differentiation and neurite outgrowth through the inactivation of MAPK phosphorylation in PC12 cells[29]. Because TBT exposure has been reported to induce neurotoxicity via ERK and p38MAPK phosphorylation in cultured rat cortical neurons[30], TBT exposure might cause cytotoxicity through the MAPK pathways. Thus, a non-genomic pathway plays a role in TBT toxicity. Indeed, the genomic target PPARγ and treatment with cycloheximide did not alter the effects of TBT (Figure S1–3). It is unlikely that transcriptional regulation is involved in NAD-IDH activity and the enhancement of neuronal differentiation. The downstream pathway of TBT-NAD-IDH should be determined in embryonic carcinoma cells.

Our data suggest that TBT regulates NAD-IDH activity through possible interaction. However, we can not conclude that it is through direct binding. Previous reports have suggested that TBT can bind to multiple target proteins, such as PPARγ, RXR, F1F0 ATP synthase and 11β-hydroxysteroid dehydrogenase (11β-HSD) type 2, with broad specificity[19,31]. For example, TBT binds the RXRα ligand-binding domain through a covalent bond between the tin atom and the Cys residue[32]. TBT also binds 11β-HSD type 2 by interacting with several Cys residues in the active site[31]. Because the ligand-binding pocket of hNAD-IDHα contains several Cys residues[33] and has enough space to accommodate TBT, TBT might bind to hNAD-IDHα via Cys residues. Future conformational analysis, including X-ray crystallography or computer simulation, and mutagenesis studies should be performed to determine whether TBT binds to hNAD-IDHα or not.

Our metabolomic analysis showed that TBT inhibited cell growth and enhanced neuronal differentiation through possible direct

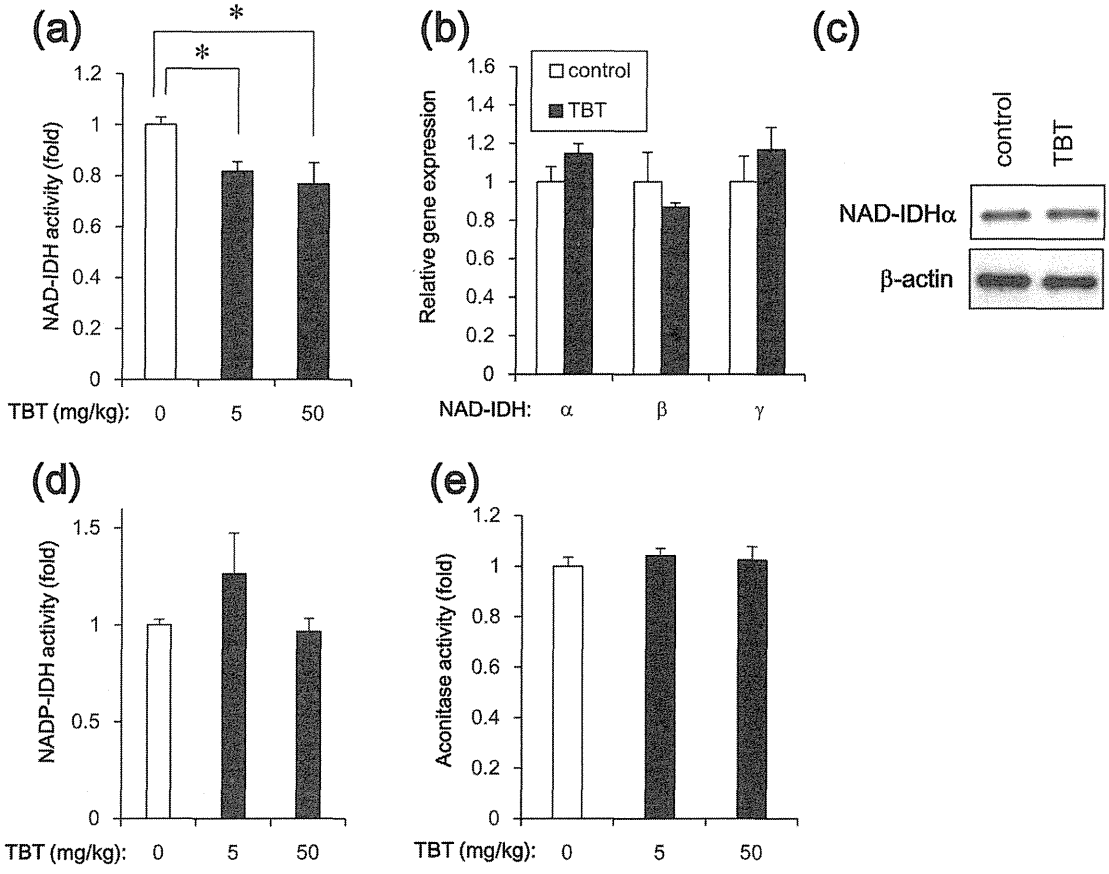

Figure 4 | NAD-IDH enzyme activity in the brain of rats orally exposed to TBT at doses of 5 and 50 mg/kg for 6 h. (a) NAD-IDH activity was determined in the brain lysates. (b) The relative expression levels of NAD-IDHα, β, and γ in rats exposed to 50 mg/kg TBT were measured using real-time PCR. The relative changes were normalized to the levels of RPL13. (c) The expression of NAD-IDHα protein was examined by western blot analysis using the anti-NAD-IDHα and anti-β-actin antibodies. Cropped blots were shown and the full-length blots were indicated in Supplementary Fig. 4. (d) NADP-IDH activity was determined in the brain lysates. (e) Aconitase activity was determined in the brain lysates. * $P < 0.05$ compared with the corresponding TBT 0 group.

inhibition of NAD-IDH activity in human embryonic carcinoma cells. Thus, comprehensive approach of non-genomic metabolic pathway might be a powerful tool to elucidate the mechanism of EDC action.

Methods

Chemicals and reagents. TBT was obtained from Tokyo Chemical Industry (Tokyo, Japan). Tin acetate (TA) and rosiglitazone were obtained from Sigma-Aldrich (St. Louis, MO, USA). All other reagents were of analytical grade and were obtained from commercial sources.

Cell culture. NT2/D1 cells were obtained from the American Type Culture Collection. The cells were cultured in Dulbecco's modified Eagle's medium (DMEM; Sigma-Aldrich) supplemented with 10% fetal bovine serum (FBS; Biological Industries, Ashrat, Israel) and 0.05 mg/ml penicillin-streptomycin mixture (Life Technologies, Carlsbad, CA, USA) at 37°C and 5% CO2. For neural differentiation, all-trans retinoic acid (RA; Sigma-Aldrich) was added to the medium twice a week at a final concentration of 10 μM.

Determination of TCA cycle metabolites. Intracellular metabolites were extracted and used for subsequent capillary electrophoresis time-of-flight mass spectrometry (CE-TOFMS) analysis, as previously described. The amounts of the metabolites were determined using an Agilent CE capillary electrophoresis system (Agilent Technologies, Waldbronn, Germany) equipped with an Agilent G3250AA LC/MSD TOF system (Agilent Technologies, Palo Alto, CA), an Agilent 1100 series isocratic HPLC pump, a G1603A Agilent CE-MS adapter kit, and a G1607A Agilent CE-electrospray ionization 53-MS sprayer kit. For system control and data acquisition, the G2201AA Agilent ChemStation software was used for CE, and the Agilent TOF (Analyst QS) software was used for the TOFMS.

Measurement of intracellular ATP levels. The intracellular ATP content was measured using the ATP Determination Kit (Life Technologies), according to the manufacturer's protocol. Briefly, the cells were washed and lysed with 0.1% Triton X-100/PBS. The resulting cell lysates were added to a reaction mixture containing 0.5 mM D-luciferin, 1 mM DTT, and 1.25 μg/ml luciferase and incubated for 30 min at room temperature. Luminescence was measured using a Wallac1420ARVO fluoroscan (Perkin-Elmer, Waltham, MA, USA). The luminescence intensities were normalized to the total protein content.

Isocitrate dehydrogenase (IDH) activity assay. IDH activity was determined using the commercial Isocitrate Dehydrogenase Activity Colorimetric Assay Kit (Biovision, Mountain View, CA, USA), according to the manufacturer's instructions. Briefly, NT2/D1 cells were lysed in an assay buffer provided in the kit. The lysate was centrifuged at 14,000 g for 15 min, and the cleared supernatant was used for the assay. NADP or NAD was used as the substrate for the NADP-IDH or NAD-IDH assay, respectively.

Real-time PCR. Total RNA was isolated from NT2/D1 cells using the TRIzol reagent (Life Technologies), and quantitative real-time reverse transcription (RT)-PCR with the QuantiTect SYBR Green RT-PCR Kit (QIAGEN, Valencia, CA, USA) was performed using an ABI PRISM 7900HT sequence detection system (Applied Biosystems, Foster City, CA, USA), as previously reported. The relative changes in the transcript amounts of each sample were normalized to the mRNA levels of ribosomal protein L13 (RPL13). The following primer sequences were used for real-time PCR analysis: human NAD-IDHα: forward, 5′-ATCGGAGGTCTCGGTGTG-3′, reverse, 5′-AGGAGGGCTGTGGGATTC-3′; human NAD-IDHβ: forward, 5′-GCCTC-AGCCGCATATCATAG-3′, reverse, 5′-GAGCAGGTGCTGAGTTCCAT-3′; human NAD-IDHγ: forward, 5′-TTAGCGGACGGAGGAATTGT-3′, reverse, 5′-CAGCCCTTCTCTGCCGT-3′; human NeuroD: forward, 5′-GGAAACGA-ACCCACTGTGCT-3′, reverse, 5′-GCCACACCAAATTCGTGGTG-3′; human Math1: forward, 5′-GTCCGAGCTGCTACAAACG-3′, reverse, 5′-GTGGTGGT-GGTCGCTTTT-3′; human RPL13: forward, 5′-CATCGTGGCTAAACAGGTAC-

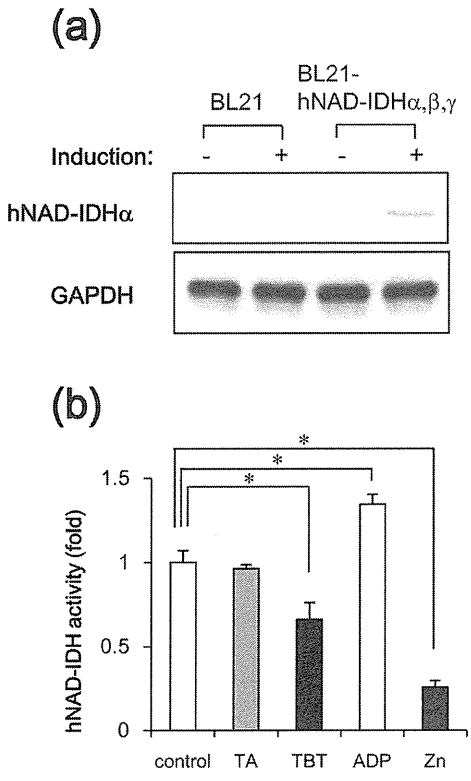

Figure 5 | Reduction of NAD-IDH enzyme activity by interaction with TBT in an E. coli expression system. (a) After the expression of pHIDHα, β, γ was induced by culturing E. coli BL21 transformants at 25°C for 20 h, crude extracts were prepared and were subjected to western blot analysis using the anti-NAD-IDHα and anti-GAPDH antibodies. Cropped blots were shown and the full-length blots were indicated in Supplementary Fig. 4. (b) After treatment with 100 nM TBT for 1 h, NAD-IDH activity was determined in the crude extracts. ADP (100 μM) and Zn^{2+} (2 mM) were used as positive and negative controls, respectively. * $P < 0.05$ compared with the corresponding control group.

TG-3′, reverse, 5′-GCACGACCTTGAGGGCAGCC-3′; rat NAD-IDHα: forward, 5′-TGGGTGTCCAAGGTCTCTC-3′, reverse, 5′-CTCCCACTGAATAGGTG-CTTTG-3′; rat NAD-IDHβ: forward, 5′-AGGCACAAGATGTGAGGGTG-3′, reverse, 5′-CAGCAGCCTTGAACACTTCC-3′; rat NAD-IDHγ: forward, 5′-TGGGCGGCATACAGTGACTA-3′, reverse, 5′-TTGGAGCTTACATGCAC-CTCT-3′; rat RPL13: forward, 5′-GGCTGAAGCCTACCAGAAAG-3′, reverse, 5′-CTTTGCCTTTTCCTTCCGTT-3′.

Aconitase activity assay. Aconitase activity was determined using the commercial Aconitase Activity Colorimetric Assay Kit (Biovision), according to the manufacturer's instructions. Briefly, NT2 cells were lysed in an assay buffer provided in the kit. The lysate was centrifuged at 14,000 g for 15 min, and the cleared supernatant was used for the aconitase assay.

NAD-IDHα knockdown experiment. Transient gene knockdown was performed using NAD-IDHα shRNA lentiviruses from Sigma-Aldrich (MISSION® shRNA) according to manufacturer's protocol. A scrambled hairpin sequence was used as a negative control. Briefly, the cells were infected with the viruses at a multiplicity of infection of 10, in the presence of 8 μg/ml hexadimethrine bromide (Sigma-Aldrich), for 24 h, and were then subjected to selection with 0.5 μg/ml puromycin for 72 h prior to functional analyses.

Tissue preparation. The present study was approved by the animal ethics committee and was conducted in accordance with the regulations on the use of living modified organisms of Hiroshima University. Male Slc:Wistar/ST rats (8 weeks old) were purchased from Japan SLC, Inc. (Shizuoka, Japan). They were housed under controlled temperature, 12 h light/dark cycle, and humidity (75 ± 5%) for at least 1 week prior to experiments. Standard pellet food and water were provided ad libitum. TBT solution (5 and 50 mg/kg body weight) was orally administered to rats. TBT was dissolved in polyethylene glycol. The whole brain was exposed by the use of fine scissors and forceps, and the frontal part of cerebral cortex was excised from the brain.

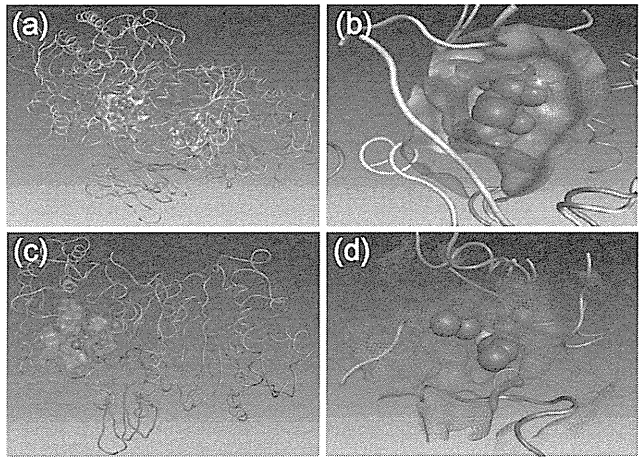

Figure 6 | *In silico* docking simulation analysis. (a) Overlaid structures of the calculated hNAD-IDHα (orange) and hNADP-IDH (cyan) homodimers bound to isocitric acid (Space-filling model). (b) The ligand binding pockets of the hNAD-IDHα (solid) and hNADP-IDH (wireframe) proteins. (c, d) Docking structure of hNAD-IDHα containing TBT (Space-filling model).

Transformation and Expression of Recombinant Human NAD-IDH Proteins in E. coli. pHIDHαβ1γ plasmid DNA (a kind gift from Dr. T. L. Huh) was used to transform E. coli BL21 (DE3) ultracompetent cells (BioDynamics, Tokyo, Japan). The colonies with positive inserts were subcultured and grown overnight at 37°C in LB medium (2 ml) supplemented with ampicillin (0.1 mg/ml). To express the enzyme, 15 ml tubes containing 2 ml of LB medium with 0.1 mg/ml ampicillin were inoculated with freshly grown E. coli cells (1% v/v), and these cultures were grown at 37°C while being shaken at 220 rpm for 4 h. The flasks were then temporarily placed in chilled water to lower the culture temperature to 25°C. Protein expression was induced in the cells by shaking at a lower speed of 140 rpm with minimal aeration at 25°C for 20 h. Then, 2 ml of the cell culture was centrifuged at 6,000 g for 15 min to separate the cells from the media, and the pellet was suspended in a total volume of 300 μl of cold assay buffer, a component of Isocitrate Dehydrogenase Activity Assay Kit. The suspended cells were subjected to 3 cycles of freeze-thaw before sonication (5 cycles of 15 sec sonication and 45 sec rest) and lysed. The cell lysate was centrifuged at 14,000 g for 15 min, and the cleared supernatant (crude extract) was separated. Recombinant human NAD-IDH activity was determined by subtracting basal activity in the crude extract from control BL21 cells.

Western blot analysis. Western blot analysis was performed as previously reported[34]. Briefly, the cells were lysed with Cell Lysis Buffer (Cell Signaling Technology, Danvers, MA, USA), and the proteins were separated by sodium dodecyl sulfate (SDS)-polyacrylamide gel electrophoresis and electrophoretically transferred to Immobilon-P (Millipore, Billerica, MA, USA). The membranes were probed with an anti-NAD-IDH (IDH3) α polyclonal antibody (1 : 1,000; Abcam, Cambridge, UK), an anti-β-actin monoclonal antibody (1 : 5,000; Sigma-Aldrich), and an anti-GAPDH monoclonal antibody (1 : 2,000; Abcam). The membranes were then incubated with secondary antibodies against rabbit or mouse IgG conjugated to horseradish peroxidase (Cell Signaling Technology). The bands were visualized using the ECL Western Blotting Analysis System (GE Healthcare, Buckinghamshire, UK), and the images were acquired using a LAS-3000 Imager (FUJIFILM UK Ltd., Systems, Bedford, UK). The density of each band was quantified using the ImageJ software (NIH, Bethesda, MD, USA).

In silico docking simulation studies. Homology modeling and docking studies of the human NAD-IDHα (hNAD-IDHα) and NADP-IDH (hNADP-IDH) homodimers were performed using Molecular Operating Environment (MOE) 2012.10. The models of hNAD-IDHα and hNADP-IDH were constructed based on the crystallographic structure of the porcine NADP-IDH homodimer (PDB: 1LWD)[35] using the standard protocols in MOE 2012.10. The docking simulations of the TBT-bound hNAD-IDHα and hNADP-IDH were carried out using ASEDock[36]. The TBT ligand was assigned in ASEDock, and the conformations were calculated using MMFF94S force field[37].

Statistical analysis. Results are shown as mean ± S.D. Statistical analysis was performed using one-way ANOVA followed by Dunnett's test. Differences at $P < 0.05$ were considered to be significant.

1. Toppari, J. *et al.* Male reproductive health and environmental xenooestrogens. *Environ. Health Perspect.* **104**, 741–803 (1996).

2. Hall, J. M. & Korach, K. S. Analysis of the molecular mechanisms of human estrogen receptors alpha and beta reveals differential specificity in target promoter regulation by xenoestrogens. *J. Biol. Chem.* **277**, 44455–44461 (2002).
3. Newbold, R. R., Padilla-Banks, E. & Jefferson, W. N. Adverse Effects of the Model Environmental Estrogen Diethylstilbestrol Are Transmitted to Subsequent Generations. *Endocrinology* **147**, s11–17 (2006).
4. Bulayeva, N. N., Gametchu, B. & Watson, C. S. Quantitative measurement of estrogen-induced ERK 1 and 2 activation via multiple membrane-initiated signaling pathways. *Steroids* **69**, 181–192 (2004).
5. Liu, D., Homan, L. L. & Dillon, J. S. Genistein acutely stimulates nitric oxide synthesis in vascular endothelial cells by a cyclic adenosine 5′-mono-phosphate-dependent mechanism. *Endocrinology* **145**, 5532–5539 (2004).
6. Watson, C. S., Alyea, R. A., Jeng, Y. J. & Kochukov, M. Y. Nongenomic actions of low concentration estrogens and xenoestrogens on multiple tissues. *Mol. Cell Endocrinol.* **274**, 1–7 (2007).
7. Bredfeldt, T. G. *et al.* Xenoestrogen-induced regulation of EZH2 and histone methylation via estrogen receptor signaling to PI3K/AKT. *Mol. Endocrinol.* **24**, 993–1006 (2010).
8. Gardlund, A. T. *et al.* Effects of prenatal exposure to tributyltin and trihexyltin on behavior in rats. *Neurotoxicol. Teratol.* **13**, 99–105 (1991).
9. Noda, T. *et al.* Teratogenicity study of tri-n-butyltin acetate in rats by oral administration. *Toxicol. Lett.* **55**, 109–115 (1991).
10. Whalen, M. M., Loganathan, B. G. & Kannan, K. Immunotoxicity of environmentally relevant concentrations of butyltins on human natural killer cells in vitro. *Environ Res.* **81**, 108–116 (1999).
11. Matthiessen, P. & Gibbs, P. E. Critical appraisal of the evidence for tributyltin mediated endocrine disruption in mollusks. *Environ. Toxicol. Chem.* **17**, 37–43 (1998).
12. McAllister, B. G. & Kime, D. E. Early life exposure to environmental levels of the aromatase inhibitor tributyltin causes masculinisation and irreversible sperm damage in zebrafish (Danio rerio). *Aquat. Toxicol.* **65**, 309–316 (2003).
13. Nishikawa, J. *et al.* Involvement of the retinoid X receptor in the development of imposex caused by organotins in gastropods. *Environ. Sci. Technol.* **38**, 6271–6276 (2004).
14. Kanayama, T., Kobayashi, N., Mamiya, S., Nakanishi, T. & Nishikawa, J. Organotin compounds promote adipocyte differentiation as agonists of the peroxisome proliferator-activated receptor gamma/retinoid X receptor pathway. *Mol. Pharmacol.* **67**, 766–774 (2005).
15. Grün, F. *et al.* Endocrine-disrupting organotin compounds are potent inducers of adipogenesis in vertebrates. *Mol. Endocrinol.* **20**, 2141–2155 (2006).
16. Cooke, G. M. Effect of organotins on human aromatase activity in vitro. *Toxicol. Lett.* **126**, 121–130 (2002).
17. Doering, D. D., Steckelbroeck, S., Doering, T. & Klingmüller, D. Effects of butyltins on human 5alpha-reductase type 1 and type 2 activity. *Steroids* **67**, 859–867 (2002).
18. McVey, M. J. & Cooke, G. M. Inhibition of rat testis microsomal 3beta-hydroxysteroid dehydrogenase activity by tributyltin. *J. Steroid Biochem. Mol. Biol.* **86**, 99–105 (2003).
19. von Ballmoos, C., Brunner, J. & Dimroth, P. The ion channel of F-ATP synthase is the target of toxic organotin compounds. *Proc. Natl. Acad. Sci. U S A* **101**, 11239–11244 (2004).
20. Yamada, S., Kotake, Y., Sekino, Y. & Kanda, Y. AMP-activated protein kinase-mediated glucose transport as a novel target of tributyltin in human embryonic carcinoma cells. *Metallomics* **5**, 484–491 (2013).
21. Vinekar, R., Verma, C. & Ghosh, I. Functional relevance of dynamic properties of Dimeric NADP-dependent Isocitrate Dehydrogenases. *BMC Bioinformatics* **13**, S2 (2012).
22. Birket, M. J. *et al.* A reduction in ATP demand and mitochondrial activity with neural differentiation of human embryonic stem cells. *J. Cell Sci.* **124**, 348–358 (2011).
23. Kim, Y. O. *et al.* Identification and functional characterization of a novel, tissue-specific NAD(+)-dependent isocitrate dehydrogenase β subunit isoform. *J. Biol. Chem.* **274**, 36866–36875 (1999).
24. Cohen, P. F. & Colman, R. F. Diphosphopyridine nucleotide dependent isocitratedehydrogenase from pig heart. Charactgerization of the active substrate and modes of regulation. *Biochemistry* **11**, 1501–1508 (1972).
25. Lemire, J., Mailloux, R. & Appanna, V. D. Zinc toxicity alters mitochondrial metabolism and leads to decreased ATP production in hepatocytes. *J. Appl. Toxicol.* **28**, 175–182 (2008).
26. Wise, D. R. *et al.* Hypoxia promotes isocitrate dehydrogenase-dependent carboxylation of α-ketoglutarate to citrate to support cell growth and viability. *Proc. Natl. Acad. Sci. U S A* **108**, 19611–19616 (2011).
27. Juang, H. H. Modulation of mitochondrial aconitase on the bioenergy of human prostate carcinoma cells. *Mol. Genet. Metab.* **81**, 244–252 (2004).
28. Gabriel, J. L., Zervos, P. R. & Plaut, G. W. Activity of purified NAD-specific isocitrate dehydrogenase at modulator and substrate concentrations approximating conditions in mitochondria. *Metabolism* **35**, 661–667 (1986).
29. Cho, S. A. *et al.* Up-regulation of Idh3alpha causes reduction of neuronal differentiation in PC12 cells. *BMB Rep.* **43**, 369–374 (2010).
30. Nakatsu, Y. *et al.* Glutamate excitotoxicity is involved in cell death caused by tributyltin in cultured rat cortical neurons. *Toxicol. Sci.* **89**, 235–242 (2006).
31. Atanasov, A. G., Nashev, L. G., Tam, S., Baker, M. E. & Odermatt, A. Organotins disrupt the 11beta-hydroxysteroid dehydrogenase type 2-dependent local inactivation of glucocorticoids. *Environ. Health Perspect.* **113**, 1600–1606 (2005).
32. le Maire, A. *et al.* Activation of RXR-PPAR heterodimers by organotin environmental endocrine disruptors. *EMBO Rep.* **10**, 367–373 (2009).
33. Kim, Y. O. *et al.* Characterization of a cDNA clone for human NAD(+)-specific isocitrate dehydrogenase alpha-subunit and structural comparison with its isoenzymes from different species. *Biochem. J.* **308**, 63–68 (1995).
34. Kanda, Y. & Watanabe, Y. Adrenaline increases glucose transport via a Rap1-p38MAPK pathway in rat vascular smooth muscle cells. *Br. J. Pharmacol.* **151**, 476–482 (2007).
35. Ceccarelli, C., Grodsky, N. B., Ariyaratne, N., Colman, R. F. & Bahnson, B. J. Crystal structure of porcine mitochondrial $NADP^+$-dependent isocitrate dehydrogenase complexed with Mn^{2+} and isocitrate. Insights into the enzyme mechanism. *J. Biol. Chem.* **277**, 43454–43462 (2002).
36. Goto, J., Kataoka, R., Muta, H. & Hirayama, N. ASEDock-docking based on alpha spheres and excluded volumes. *J. Chem. Inf. Model.* **48**, 583–590 (2008).
37. Halgren, T. A. MMFF VI. MMFF94s option for energy minimization studies. *J. Comput. Chem.* **20**, 720–729 (1999).

Acknowledgments

We thank Ms. Mami Kohno, Mr. Kyoichi Masuda, and Ms. Saki Tanaka (Graduate School of Biomedical and Health Sciences, Hiroshima University) for technical assistance in the animal experiment. This work was supported by a Grant-in-Aid for Scientific Research from the Ministry of Education, Culture, Sports, Science, and Technology, Japan (#23590322 to Y.K.), a Health and Labour Sciences Research Grant from the Ministry of Health, Labour and Welfare, Japan (Y.K.), and a grant from the Smoking Research Foundation (Y.K.).

Author contributions

S.Y. performed most of the experiments. Y.Ka. planned the project. S.Y., Y.S. and Y.Ka. wrote the manuscript. Y.Ko. performed the animal experiments. Y.D. and M.K. performed *In silico* docking simulation analysis. All authors reviewed the manuscript.

Additional information

Supplementary information accompanies this paper at http://www.nature.com/scientificreports

Competing financial interests: The authors declare no competing financial interests.

How to cite this article: Yamada, S. *et al.* NAD-dependent isocitrate dehydrogenase as a novel target of tributyltin in human embryonic carcinoma cells. *Sci. Rep.* **4**, 5952; DOI:10.1038/srep05952 (2014).

Bioorganic & Medicinal Chemistry Letters 23 (2013) 4292–4296

Contents lists available at SciVerse ScienceDirect

Bioorganic & Medicinal Chemistry Letters

journal homepage: www.elsevier.com/locate/bmcl

Development of stapled short helical peptides capable of inhibiting vitamin D receptor (VDR)–coactivator interactions

Yosuke Demizu [a,*], Saori Nagoya [a], Manami Shirakawa [a], Megumi Kawamura [a,b], Nanako Yamagata [a], Yukiko Sato [a], Mitsunobu Doi [c], Masaaki Kurihara [a,b,*]

[a] Division of Organic Chemistry, National Institute of Health Sciences, 1-18-1 Kamiyoga, Setagaya, Tokyo 158-8501, Japan
[b] Graduate School of Bioscience and Biotechnology, Tokyo Institute of Technology, Yokohama 226-8501, Japan
[c] Osaka University of Pharmaceutical Sciences, Osaka 569-1094, Japan

ARTICLE INFO

Article history:
Received 29 April 2013
Revised 27 May 2013
Accepted 1 June 2013
Available online 10 June 2013

Keywords:
Vitamin D receptor
VDR–coactivator interaction inhibitor
Stapled helical peptide
Protein–protein interaction

ABSTRACT

We synthesized stapled helical leucine-based peptides (**DPI-01-07**) containing 2-aminoisobutyric acid and a covalent cross-linked unit as inhibitors of vitamin D receptor (VDR)–coactivator interactions. The effects of these peptides on the human VDR were examined in an inhibition assay based on the receptor cofactor assay system, and one of them, **DPI-07**, exhibited potent inhibitory activity (IC_{50}: 3.2 μM).

The vitamin D receptor (VDR), a nuclear receptor (NR), regulates various biological actions such as calcium uptake, cell proliferation and differentiation, and immune modulation. 1α,25-Dihydroxyvitamin D_3 [1α,25$(OH)_2D_3$] is an endogenous VDR ligand and has also been demonstrated to regulate these biological events via the VDR.[1,2] Therefore, agonistic 1α,25$(OH)_2D_3$ derivatives (secosteroidal VDR ligands) and non-secosteroidal VDR ligands are considered to be therapeutic candidates for the treatment of osteoporosis, various types of rickets, secondary hyperparathyroidism, psoriasis, autoimmune diseases, and cancer.[3–10] On the other hand, antagonistic VDR ligands are considered to be useful for the treatment of conditions involving hypersensitivity to 1α,25$(OH)_2D_3$, such as

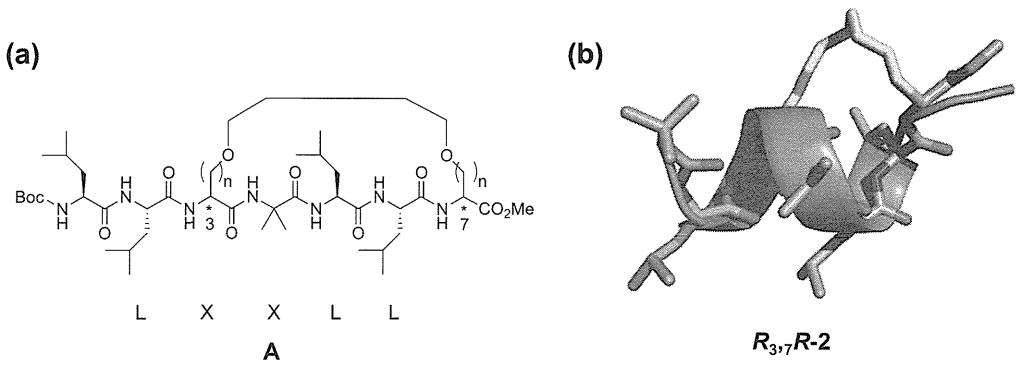

Figure 1. (a) Chemical structure of the stapled heptapeptides. (b) X-ray structure of the stapled heptapeptide $R_{3,7}$**R-2**. The covalent side chain is shown in green. The nomenclature $R_{3,7}R$ refers to a peptide with *R* configurations at its 3rd and 7th positions.

* Corresponding authors. Tel.: +81 3 3700 1141; fax: +81 3 3707 6950.
E-mail addresses: demizu@nihs.go.jp (Y. Demizu), masaaki@nihs.go.jp (M. Kurihara).

0960-894X/$ - see front matter © 2013 Elsevier Ltd. All rights reserved.
http://dx.doi.org/10.1016/j.bmcl.2013.06.002

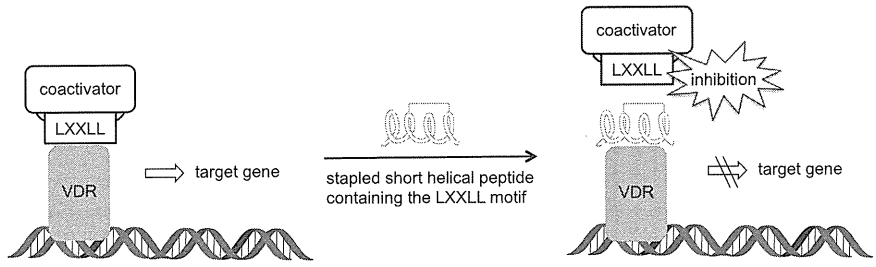

Figure 2. Illustration of the mechanism by which the stapled short helical peptides inhibited VDR–coactivator interactions.

Paget's disease of bone,[11] which results in an abnormal bone architecture. To date, several secosteroidal VDR antagonists have been developed.[10] In addition, small molecules[12–14] and peptides[15–17] containing the consensus sequence LXXLL [L: leucine (Leu), X: any amino acid residue] have been demonstrated to inhibit VDR–coactivator interactions. Therefore, they are also considered to be drug candidates for reducing VDR-mediated transactivation. In order to bind to the VDR, small molecules/peptides must contain three Leu residues or Leu mimics.[15–17] Furthermore, small peptides have to have an α-helical structure to efficiently interact with the VDR. It is sometimes difficult to form stable α-helices in short peptides. However, α,α-disubstituted α-amino acids (dAAs)[18–20] and a covalent cross-linking system[21–24] have been demonstrated to be useful for stabilizing the helical structures of such peptides. Especially, 2-aminoisobutyric acid (Aib) has been used as a strong helical promoter.[25–28] The covalent cross linker at the *i* and *i*+3 positions on peptides has been found to be also useful for the helix-stabilization strategy, as reported by Grubbs and Verdine.[22,29] Recently, we reported that the combined use of 2-

Table 1
IC_{50} values of peptides **DPI-01-07** against human VDR–cofactor interactions according to a receptor cofactor assay system[a]

Entry	Peptide	IC_{50} (μM)
1	**H-$S_{3,7}S$-2-OH (DPI-01)**	610
2	**H-$S_{3,7}R$-2-OH (DPI-02)**	430
3	**H-$R_{3,7}S$-2-OH (DPI-03)**	610
4	**H-$R_{3,7}R$-2-OH (DPI-04)**	600
5	**H-$hS_{3,7}S$-2-OH (DPI-05)**	520
6	**H-$hS_{3,7}hS$-2-OH (DPI-06)**	220
7[b]	**H-$hS_{3,7}hS^{dOH}$-2-OH (DPI-07)**	3.2

[a] The EC_{50} value of the positive control, 1α,25(OH)$_2$D$_3$, was 7.7 nM.
[b] An isomeric mixture of **DPI-07** was examined in the assay.

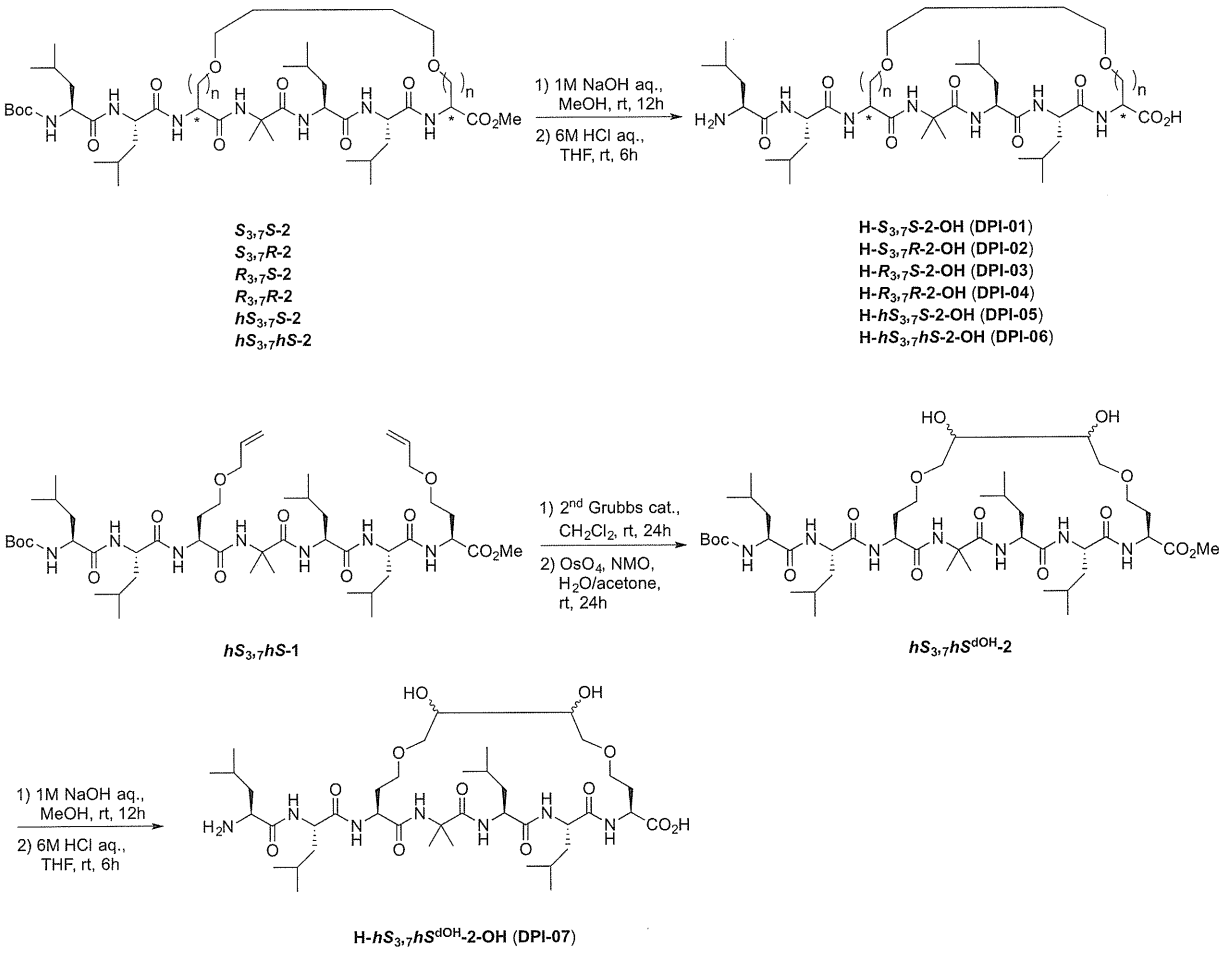

Scheme 1. Synthesis of the stapled heptapeptides. The nomenclature ***hS*** indicates a L-homoserine (L-Hse) derivative.